Title: Desert Cucurbit Microbiomes: Spatiotemporal Dynamics and Functional Adaptations

Miranda Procter[1], Biduth Kundu[1], Naganeeswaran Sudalaimuthuasari[2], Raja S. AlMaskari[1], Iltaf Shah[3], Shaima Alnuaimi[1], Farah Husain[1], Khawla Aldhaheri[1], Khaled M. Hazzouri[2,*] and Khaled M. A. Amiri[1,2*]

1 Department of Biology, College of Science, United Arab Emirates University, Al Ain P.O. Box. 15551, United Arab Emirates

2 Khalifa Center for Genetic Engineering and Biotechnology, United Arab Emirates University, Al Ain P.O. Box. 15551, United Arab Emirates

3 Department of Chemistry, College of Sciences, United Arab Emirates University, Al Ain, UAE

*Correspondence: k.amiri@uaeu.ac.ae

khaled_hazzouri@uaeu.ac.ae

Author email and ORCID details:

Miranda Procter - 202190131@uaeu.ac.ae, ORCID - https://orcid.org/0000-0002-0054-2112; Biduth Kundu - biduth.k@uaeu.ac.ae, Naganeeswaran Sudalaimuthuasari - naganeeswaran@uaeu.ac.ae, ORCID - https://orcid.org/0000-0002-4626-7515; Raja S. AlMaskari - R.almeskari@uaeu.ac.ae; Iltaf Shah - altafshah@uaeu.ac.ae; Shaima Alnuaimi - 202005791@uaeu.ac.ae; Farah Husain - 202051116@uaeu.ac.ae; Khawla Aldhaheri - 202000527@uaeu.ac.ae; Khaled M. Hazzouri - khaled_hazzouri@uaeu.ac.ae, ORCID - https://orcid.org/0000-0002-9346-3906; Khaled M. A. Amiri - k.amiri@uaeu.ac.ae, ORCID - https://orcid.org/0000-0003-3240-2736.

Abstract

Aridification and climate stress threaten global plant productivity, but the survival strategies of desert plants remain only partly understood. In this study, we examined how the microbiome of *Citrullus colocynthis*, a hardy desert cucurbit valued for its ecological and medicinal benefits, may influence the plant's ability to withstand harsh conditions. Using 16S rRNA amplicon sequencing, shotgun metagenomics, and culture-based methods, we analyzed microbiome changes across two regions of the UAE during the rainy and dry seasons. Leaf and root bacterial communities showed clear seasonal shifts, with greater richness in winter and higher evenness in summer, while soil microbiomes remained stable. Dominant bacterial groups, Actinomycetota and Pseudomonadota, varied seasonally, indicating trade-offs between stress tolerance and metabolic flexibility. Fungal communities (mainly Ascomycota and Basidiomycota) were stable at the phylum level but reorganized by order between seasons; archaeal populations showed little change. Among 24 cultured bacterial isolates, including three potential new species, we identified multiple stress tolerance and plant growth–promoting traits. Genomic data revealed biosynthetic clusters for antimicrobial and stress-protective functions, as well as adaptation genes in *Pseudomonas orientalis*. These results demonstrate that the dynamic, functionally diverse microbiome of *C. colocynthis* enhances its resilience to desert stress, offering potential for arid-land agriculture.

Keywords: *Citrullus colocynthis*, desert microbiome, plant-microbe interactions, stress tolerance

1. Background

Climate stressors, including heat, drought, and salinity, are increasingly tightening their hold on global agriculture, making resilience a necessity rather than just an aspiration (Vandenkoornhuyse et al., 2015; (IPCC), 2023). In deserts, survival often depends not only on plant physiology but also significantly on partnerships with microbes that support tolerance to water scarcity, extreme temperatures, and nutrient deficiency (Rodriguez and Redman, 2008; Alsharif et al., 2020; Glick and Gamalero, 2021; Shah et al., 2021; Zhang and White, 2021). However, the ways in which these plant–microbiome partnerships function across different spaces and seasons remain only partially understood. Research across systems shows that plant-associated communities can change notably between wetter and drier periods, often with greater shifts in leaves and roots compared to nearby soils (Edwards et al., 2018; Landesman et al., 2019; Howe et al., 2023; Argiroff William et al., 2024; Zhang et al., 2024). Gaining a clear understanding of these dynamics is essential for moving from simple observation to uncovering mechanisms.

Citrullus colocynthis offers a unique opportunity to explore these questions firsthand in real-world conditions. This desert cucurbit is valued for its medicinal and agricultural potential (Dane et al., 2006; Hussain et al., 2014; Silva and Hussain, 2017; Meybodi, 2020; Abushamleh et al., 2022) and exhibits notable physiological adaptations to extreme temperatures (Elnaggar et al., 2024). Previous studies on *C. colocynthis* and its microbial partners help shape our understanding: isolation-based research has identified disease-suppressive and growth-promoting activities among endophytes and rhizobacteria (Al-Shuaibi et al., 2023), antibacterial properties in endophytic actinobacteria (Ali et al., 2022a), and tissue- and site-specific diversity of fungal endophytes (Sohrabi et al., 2024). Broader desert surveys that included *C. colocynthis* have

68 occasionally detected limited fungal diversity (Noor et al., 2021). Moving beyond culture-based
69 efforts, we conducted an initial study on the bacterial component of the microbiome and identified
70 various bacteria associated with the plant, many of which are known to promote plant growth
71 (Procter et al., 2022). Subsequent culture-based research further emphasized that rhizosphere
72 isolates can possess multiple traits supporting plant growth under arid conditions (Dekak et al.,
73 2025). Collectively, these studies motivate a more integrated approach to understanding the *C.*
74 *colocynthis* holobiont, one that links community changes with functional capabilities.
75
76 The holobiont perspective considers plants and their microbes as an adaptive system where
77 performance results from interactions among partners (Hassani et al., 2018; Mesny et al., 2023).
78 In this context, differences in lifestyle between plant-associated and free-living microbes become
79 essential. For example, plant-associated *Pseudomonas* often show genomic features related to
80 rhizosphere competence (such as antibiotic and siderophore pathways, and the ability to trigger
81 systemic resistance), while many beneficial plant bacteria produce the auxin indole-3-acetic acid
82 (IAA) through tryptophan-based routes, influencing development and defense (Loper et al., 2012;
83 De Vrieze et al., 2020; Saati-Santamaría et al., 2022; Tang et al., 2023a). These principles suggest
84 testable connections between seasonal fluctuations in community composition, habitat specificity
85 (leaf, root, soil), and functions vital for stress tolerance.
86
87 Guided by this framework, our goal was to determine whether the spatiotemporal dynamics of the
88 microbiome and microbial traits align with the ecological needs of a desert plant. We examined
89 the microbiome of *C. colocynthis* using 16S rRNA amplicon sequencing and shotgun
90 metagenomics of plants and surrounding soils sampled in two emirates of the United Arab

Emirates (UAE) during rainy and dry seasons. We then isolated endophytic strains from leaf and root tissues, sequenced their genomes, and assessed stress tolerance and plant growth–promoting traits, including phytohormone production and antimicrobial activity in vitro. Along with previous studies, our results together provide a clear picture of how the *C. colocynthis* holobiont may support resilience in dry environments.

2. Methods

2.1. Sample collection

Leaf, root, root zone, and bulk soil samples were collected from three *C. colocynthis* plants in natural populations at Al Ain city (24°27'50.8" N 55°38'37.1" E) and Ras Al Khaimah (RAK) emirate (25°33'11.7" N 55°53'18.9" E), UAE, as described previously (Procter et al., 2022). Thus, the study included three biological replicates and three technical replicates for each biological replicate, per sample type, per season. The locations were selected due to their different rainfall patterns and geography. Endophytic bacteria were isolated from freshly collected leaf and root samples from the Al Ain site in January 2022, and samples from March and August 2022 were used for microbiome analysis.

2.2. Amplicon Profiling and Metagenomic Analyses

2.2.1. DNA extraction

Root and leaf samples were surface sterilized (1% bleach, 3 min; two sterile water washes; 70% ethanol, 3 min; six sterile water washes) (Sahu et al., 2022). The final wash water was plated on nutrient agar (NA, HiMedia, Mumbai, India) and potato dextrose agar (PDA, Conda Lab, Madrid,

Spain) to assess sterility. DNA was extracted using the XpressDNA Plant Kit (MagGenome, India) according to the manufacturer's protocol. However, the root samples were incubated at 56 °C for an additional 30 minutes during the lysis step. DNA was extracted from 2g of soil using a combination of the DNeasy PowerSoil Pro (Qiagen, Hilden, Germany) and XpressDNA Soil Kit (MagGenome, India). These extractions were repeated and pooled (for the same biological replicate, i.e., technical replicates were pooled) until enough DNA was obtained for the respective sequencing strategies. The quality and quantity of the extracted DNA were confirmed as previously described (Procter et al., 2022).

2.2.2. 16S rRNA Gene-based Microbial Profiling

16S rRNA amplicon sequencing validated DNA suitability and provided a preliminary comparison of samples across locations and seasons, . The DNA samples were amplified, trimmed, and quality assessed as described previously (Procter et al., 2022). We used the ASV file for analyses with MicrobiomeAnalyst2 (Lu et al., 2023) and the updated Greengenes database (McDonald et al., 2024). Alpha diversity was assessed using Shannon (Shannon, 1948) and Chao1 (Chao, 1984) indices, and NMDS was employed for beta diversity analysis, which guided subsequent metagenomic analysis.

2.2.3. Metagenome-based Microbial Profiling

Shotgun metagenomic sequencing was performed on an Illumina NovaSeq PE150 (150 bp paired-end) platform, generating approximately 20 GB of raw data per sample. The quality of the PE reads was assessed with FastQC v.0.11.9 (Andrews, 2010). Low-quality reads and adapter sequences were removed using Trimmomatic v.0.39 (Bolger et al., 2014). The trimmed reads were

then used for metagenome profiling with Kraken 2, a standard k-mer based method for taxonomic classification of metagenomic reads (Wood et al., 2019).

2.2.4. Seasonal and Geographic Comparisons of the Bacterial Microbiome

Kraken-based metagenomic reports and sample metadata were used to compare bacterial communities in leaf and root tissues across seasons and locations. Although the archive contained other sample classes, this analysis was restricted to leaf and root samples (24 profiles total). All viral and non-bacterial assignments were excluded before downstream analysis. Kraken lineage-style abundance reports were parsed, bacterial terminal assignments were retained, and profiles were collapsed to a comparable genus-level representation for cross-sample analysis. Relative-abundance tables were then used for diversity and community analyses.

Alpha diversity was summarized using observed bacterial genera, Shannon diversity, and Pielou evenness (Pielou, 1966). Bray-Curtis dissimilarities (Bray and Curtis, 1957) quantified compositional turnover, and metric multidimensional scaling were used for ordination. Seasonal effects within each location-tissue subgroup were tested using PERMANOVA (Anderson, 2001). Because each subgroup contained only three winter and three summer replicates, seasonal changes in alpha diversity and genus-level relative abundance were evaluated with exact two-sided Mann-Whitney tests and Cliff's delta effect sizes, with false discovery rate correction applied within each test family. Interpretation emphasized effect sizes and multivariate shifts more than adjusted taxon-level p-values alone.

2.2.5. Functional Profiling using Root Samples

Functional profiling was restricted to root samples which is essential because the rhizosphere provides a more stable, manageable environment for beneficial microbes to directly enhance plant

157 water/nutrient acquisition and survival against severe abiotic stresses. Analyses used HUMAnN
158 output, including gene-family, pathway-abundance, pathway-coverage tables, and merged
159 relative-abundance matrices. HUMAnN estimates microbial pathway abundance by mapping
160 reads to pangenome and protein reference databases, providing robust community-scale functional
161 reconstruction (Franzosa et al., 2018; Beghini et al., 2021). The merged pathway abundance matrix
162 was the main input for downstream analyses.
163 Unstratified pathways summarized community-wide functions for ordination and seasonal
164 comparisons, while stratified rows identified contributing taxa. Pathway names with provenance
165 tags (e.g., plants, yeast, archaea) were retained if linked to MetaCyc reactions, interpreted as shared
166 pathways. Analyses focused on enriching endophytic taxa involved in exopolysaccharide
167 production, biofilm formation, one-carbon metabolism, amino-acid biosynthesis, cofactor salvage,
168 and redox buffering, all relevant to the *C. colocynthis* habitat.
169

170 ## *2.3. Bacterial culture identification and genome annotation*

171 ### 2.3.1. Isolation

172 Root and leaf samples were surface-sterilized as previously described. Tissues were homogenized
173 in 10 mL of sterile water, diluted 1:10, and stored at 4°C for 7 days before being serially diluted 6
174 times. The last three dilutions were plated on half-strength NA and starch nitrate agar (SNA)
175 supplemented with cycloheximide (100 mg/L), dried upright at room temperature, and then
176 incubated inverted at 28°C. Colonies were sub-cultured until pure. Cultures were grouped by
177 morphotype and maintained on Luria-Bertani (LB) agar (HiMedia, Mumbai, India) without
178 antibiotics.

179

180 2.3.2. Initial identification

181 Pure cultures were grown in LB broth at 30°C with agitation at 150 rpm for 48 hours, and DNA
182 was extracted using the Xpress DNA Bacteria Kit (MagGenome) per the manufacturer's protocol.
183 DNA quantity and quality were assessed as previously described (Procter et al., 2022). The 16S
184 rRNA gene was used for initial identification and amplified with primers 27F
185 (AGAGTTTGATCMTGGCTCAG) and 1492R (GGTTACCTTGTTACGACTT) in 20 µL
186 reactions using DreamTaq Polymerase (Thermo Fisher Scientific, California, USA). PCR products
187 were analyzed on a 1% agarose gel and purified using ExoSAP-IT (Applied Biosystems, Thermo
188 Fisher Scientific). Cycle sequencing was performed using the BigDye Terminator v3.1 kit
189 (Applied Biosystems) with the same primers and analyzed on an Applied Biosystems 3500 Series
190 Genetic Analyzer. Consensus sequences from forward and reverse primers were generated with
191 BioEdit (Hall, 1999). Homologous sequences were identified via BLAST
192 (https://blast.ncbi.nlm.nih.gov/Blast.cgi) using blastN.

193

194 2.3.3. Whole-genome sequencing (WGS)

195 The same DNA extracted for initial identification was used, and WGS libraries (Illumina and ONT,
196 respectively) were prepared. Raw data were trimmed, a hybrid genome assembly was performed,
197 and gene annotation was completed as described by (Elmahi et al., 2021). Assembly was conducted
198 with Unicycler v.0.4.8 (Wick et al., 2017), MaSuRCA v.4.0.4 (Zimin et al., 2013), and CANU
199 v.2.2 for hybrid assembly. The assembled genomes were corrected for errors using Pilon (Walker
200 et al., 2014). Assembly completeness was validated with BUSCO (Seppey et al., 2019). The
201 assembled genome sequences were uploaded to the Type (Strain) Genome Server (TYGS)

(https://tygs.dsmz.de/) for precise identification. For isolates suspected to be new species, ANI scores between the genome and the closest relative (based on TYGS and BLAST) were calculated using CJ Bioscience's online Average Nucleotide Identity (ANI) calculator (Yoon et al., 2017). An ANI score of ≥ 96% indicates the same species, ≥ 99% indicates the same strain, and less than 96% suggests a new species.

2.3.4. Functional annotation

The assembled genomes were annotated in NCBI GenBank using the NCBI Prokaryotic Annotation Pipeline (Tatusova et al., 2016). Protein similarities were identified with BlastP against UniProt (Ewens and Grant, 2001; UniProt, 2023). Metabolic pathway genes were detected via KEGG-KAAS using GHOSTZ (Moriya et al., 2007) and mapped with KEGG Mapper. The COG classification utilized COGclassifier v.1.0.5. Gene Ontology data were obtained from UniProt. Biosynthetic gene clusters (BGCs) were annotated with antiSMASH 7.0 (Blin et al., 2023), and OrthoVenn3 (Sun et al., 2023) was used to compare orthologous clusters with reference genomes.

2.4. Culture-based Biochemical Assays and Stress Tolerance

2.4.1. Stress tolerance

Cultures grown on LB agar for one week served as the inoculum for the assays. Drought tolerance was tested by adding 10-30% PEG8000 (Muthuraja, 2023 #63) to LB broth, with incubation at 30°C and 150 rpm overnight. OD600 readings classified isolates as sensitive (≥0.29), moderately tolerant (0.3–0.39), or tolerant (≤0.4). Salinity tolerance was assessed on LB agar with 2-12% NaCl (w/v) in 2% increments, and the plates were incubated as above. Heat tolerance was tested at 22°C and 30–55°C in 5°C increments; plates with no growth after 7 days were kept at 22°C to

assess recovery. pH tolerance was determined using LB broth, adjusted from pH 4 to 10 with 1 M HCl or NaOH, and incubated as described.

2.4.2. Qualitative enzyme activity assays

The inoculum was prepared as described under stress tolerance. Screening media included skim milk agar (HiMedia) for nitrogen dissolution (Li et al., 2022), Pikovskaya's agar (HiMedia) with 5% bromophenol blue for phosphate solubilization, M9 salts (HiMedia) with 1% (w/v) citrus pectin for pectinase, or 1% CMC for cellulase, starch agar for amylase (HiMedia), Aleksandrow agar (HiMedia) for potassium solubilization, and nitrogen-free Dworkin and Foster's salts minimal agar (DF; (Dworkin and Foster, 1958)) with 2 g $(NH_4)_2SO_4$ or 3 mM ACC (Sigma-Aldrich, Maryland, USA) as sole nitrogen source. After incubation at 35°C for up to seven days in triplicate, the pectinase, amylase, and cellulase plates were stained with Gram's iodine or Congo red to visualize clear zones. IAA was detected by incubating LB broth with 2 g/L L-tryptophan at 37°C with shaking (150 rpm) for 24 h, followed by the addition of Salkowski's reagent (2:1) and incubation in the dark for 30 min (Saeed, 2024 #64). A red color indicated the presence of IAA.

2.4.3. Phytohormone production

Spent LB culture medium was used for LC-MS/MS analysis to examine if the bacteria can produce phytohormones related to PGP. We tested for 6-benzylaminopurine (6-BA), naphthalene acetic acid (Shah et al.), IAA, salicylic acid (SA), indole-3-butyric acid (IBA), isopentenyl adenine (iPA), gibberellic acid (GA3), and abscisic acid (ABA), based on available standards. The methodology followed is described in the Appendix.

2.5. Pangenome analysis of Pseudomonas orientalis

Whole-genome sequences for *P. orientalis*, were downloaded from NCBI in FASTA format, and used alongside our genome sequence for isolate B20 to create a pangenome dataset. Annotations were generated with Prokka v.5.30.2 (Kimbrel et al., 2022), and completeness and quality assessed using BUSCO. High-quality GFF3 files were input into Roary (Page et al., 2015) (BLASTP identity ≥ 95%) for pan-genome analysis, producing a gene presence/absence matrix visualized in R (heatmap2; (R Core Team, 2024)). Pan-genome openness was modeled with the power-law equation $K = \kappa \cdot n - \gamma$ (Matthews et al., 2024); $\gamma > 1$ indicates a closed pan-genome, $0 < \gamma \leq 1$ an open one. TWILIGHT (Horesh et al., 2021) identified lineage-specific accessory gene adaptations in complete genomes of free-living and plant-associated strains (including B20). Genes were grouped into core, accessory, intermediate, and unique categories, and their phylogenetic mapping was used to detect selection and ecological associations. Pan-genome fluidity and diversity (pairwise diversity π, Watterson's θ) were estimated with ANGSD (Korneliussen et al., 2014), using *P. aeruginosa* mutation rates (10^{-11}). Effective population size (Ne) was calculated as $\theta = 2Ne\mu$. Statistical differences between lifestyles were tested with the Wilcoxon test (R; $P < 0.05$).

3. Results

3.1. Seasonal dynamics of microbial communities reflect environmental changes

3.1.1. Amplicon-based diversity reveals tissue- and season-dependent community structure.

Amplicon sequencing produced 3,302,346 reads from leaf and root samples, grouped into 2,437 ASVs and rarefied to 115,691; soils yielded 1,535,076 reads and 19,729 ASVs, rarefied to 40,741. Diversity across plant tissues varied significantly with season. Species richness, estimated by

Chao1, decreased noticeably from winter to summer in both leaves (winter 38.5 ± 4.7, summer 3.8 ± 1.7; Mann-Whitney U = 36, p = 0.005) and roots (winter 32.3 ± 7.7, summer 9.2 ± 3.3; U = 36, p = 0.005). Shannon diversity showed a contrasting pattern between tissue types: root communities were significantly more diverse in summer than winter (winter 0.423 ± 0.098, summer 0.713 ± 0.091; U = 36, p = 0.002), while leaf communities showed no significant seasonal change in evenness despite their reduced richness (U = 27, p = 0.180), suggesting that the remaining leaf-associated taxa maintained a stable relative distribution across seasons. Roots harbored significantly greater Shannon diversity than leaves overall (U = 122, p = 0.004), consistent with roots supporting a more evenly distributed microbiome regardless of season (Figure 1A–B). Beta diversity analysis based on Jensen-Shannon divergence confirmed strong seasonal structuring of plant-associated communities, with season explaining 71.9% of total compositional variation (PERMANOVA: pseudo-F = 14.24, R^2 = 0.719, p = 0.0008). Tissue type accounted for a smaller but still significant proportion of variation (pseudo-F = 4.72, R^2 = 0.179, p = 0.041), while sampling location had no significant effect on community composition (pseudo-F = 0.07, p = 0.806). This indicates that seasonal dynamics and tissue identity, rather than geography, are the main factors shaping plant-associated microbial community structure. NMDS ordination confirmed clear seasonal separation and tight within-season clustering across both tissue types and locations (stress = 0.016; Figure 1C).

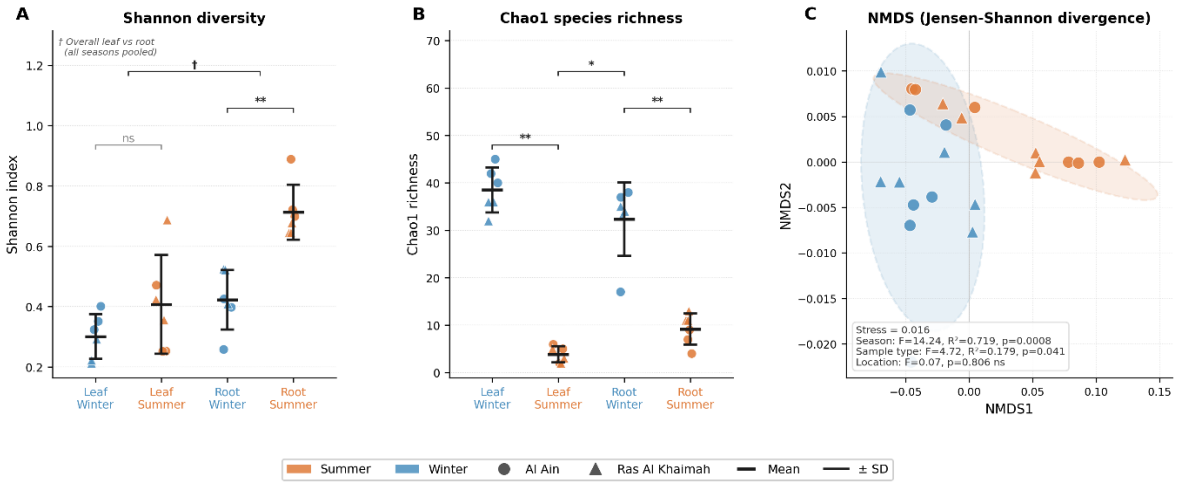

Figure 1. Alpha and beta diversity of plant tissue-associated microbial communities. (A) Shannon diversity index and (B) Chao1 species richness of leaf- and root-associated communities across seasons and sampling locations. Individual points represent biological replicates (n = 6 per group; 3 Al Ain, 3 Ras Al Khaimah); horizontal bars and error bars indicate mean ± SD. Significance brackets denote pairwise Mann-Whitney U test results (** $p < 0.01$; * $p < 0.05$; ns, not significant). † indicates the overall comparison between leaf and root communities pooled across seasons ($U = 122$, $p = 0.004$ for Shannon; $U = 3$, $p = 0.020$ for Chao1 in summer only). (C) Non-metric multidimensional scaling (NMDS) ordination of community composition based on Jensen-Shannon divergence distances calculated at species level. Dashed ellipses represent 95% confidence intervals around seasonal group centroids. PERMANOVA results (9,999 permutations) are shown in the annotation box. Colour indicates season (orange, summer; blue, winter); marker shape indicates sampling location (circle, Al Ain; triangle, Ras Al Khaimah).

In contrast, soil microbial communities showed much greater stability across different seasons. Root zone soil Shannon diversity did not significantly differ between winter and summer at either site (overall: winter 4.479 ± 0.294, summer 4.450 ± 0.122; $U = 24$, $p = 0.394$; Al Ain: $U = 9$, $p = 0.100$; RAK: $U = 2$, $p = 0.400$), and species richness estimated by Chao1 remained similarly stable (overall: winter 395.9 ± 46.5, summer 376.7 ± 43.0; $U = 26$, $p = 0.240$). Root zone soils supported significantly higher species richness than bulk soils (386.3 ± 43.9 vs 313.1 ± 41.3; $U = 33$, $p = 0.031$), although bulk soils tended to have higher Shannon evenness (4.686 ± 0.053 vs 4.465 ± 0.215; $U = 4$, $p = 0.048$). However, bulk soil sampling was limited to RAK and included only three samples (Figure 2A–B), so these comparisons are exploratory and should be interpreted

accordingly. Beta diversity analysis confirmed no seasonal variation in soil communities (PERMANOVA: pseudo-F = 0.363, p = 0.865), contrasting sharply with the clear seasonal pattern observed in plant tissues. Communities in root zone and bulk soil differed in composition (pseudo-F = 10.722, R^2 = 0.541, p = 0.001), aligning with the known influences of root exudates and rhizosphere activity on soil microbial assembly. NMDS ordination showed no obvious seasonal clustering but did reveal a clear separation between root zone and bulk soil samples (stress = 0.086; Figure 2C).

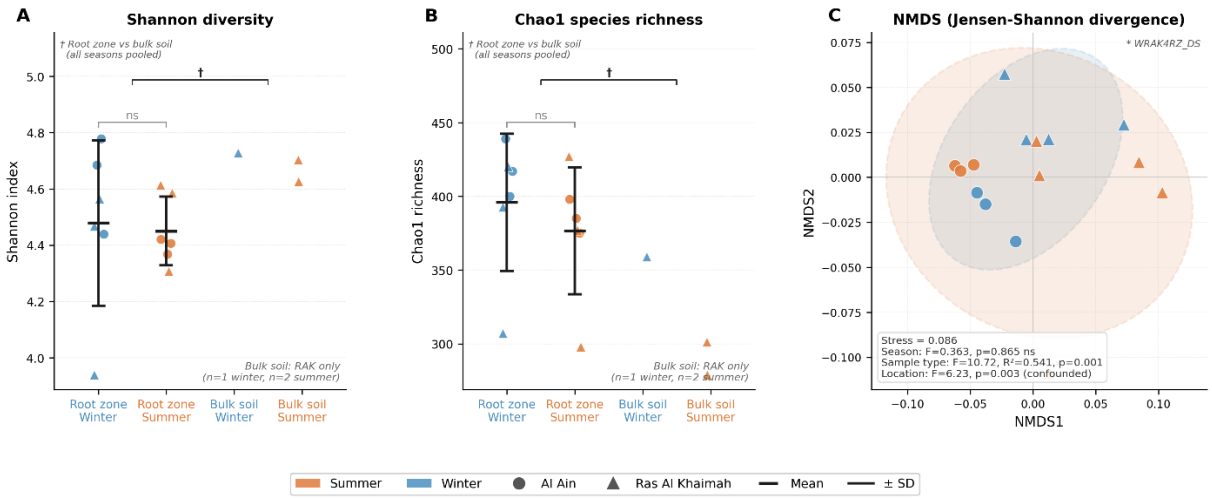

Figure 2. Alpha and beta diversity of soil microbial communities. (A) Shannon diversity index and (B) Chao1 species richness of root zone and bulk soil communities across seasons. Root zone samples: n = 6 per season (3 Al Ain, 3 Ras Al Khaimah); bulk soil samples: n = 1 (winter) and n = 2 (summer), Ras Al Khaimah only. For root zone groups, horizontal bars and error bars indicate mean ± SD; mean and SD are not shown for bulk soil groups owing to insufficient replication. Significance brackets denote Mann-Whitney U test results (ns, not significant; * $p < 0.05$). † indicates the comparison between root zone and bulk soil communities pooled across seasons, which should be interpreted with caution, given the limited bulk soil sample size and single-location sampling. (C) NMDS ordination of community composition based on Jensen-Shannon divergence distances at the species level. Dashed ellipses represent 95% confidence intervals around seasonal group centroids. PERMANOVA results (9,999 permutations) are shown in the annotation box; the location result is noted as confounded with sample type, as all Al Ain samples are root zone, while Ras Al Khaimah includes both root zone and bulk soil. * denotes sample WRAK4RZ_DS, which showed an atypical ordination position and was retained in all analyses.

Color indicates season (orange, summer; blue, winter); marker shape indicates sampling location (circle, Al Ain; triangle, Ras Al Khaimah).

3.1.2. Metagenomic profiling corroborates seasonal restructuring and highlights root community turnover.

Shotgun metagenomic sequencing and Kraken2 taxonomic classification were used to characterize bacterial communities at the genus level across leaf and root tissue samples from both sites and seasons (n = 3 per location–tissue–season subgroup; 24 profiles total). Alpha diversity was summarized as observed bacterial genera, Shannon diversity, and Pielou evenness, with seasonal comparisons evaluated using Mann-Whitney tests and Cliff's delta effect sizes; full statistical outputs are provided in Supplementary Table S1.

Leaf-associated communities showed no meaningful seasonal change in Shannon diversity, observed genera, or evenness at either site. Root communities, by contrast, showed consistent summer declines in Shannon diversity and evenness at both sites, while observed genus richness remained stable. Shannon diversity decreased from 5.924 ± 0.194 to 4.784 ± 1.434 in Al Ain roots ($U = 7$, Cliff's $\delta = -0.556$, $p = 0.4$) and from 5.962 ± 0.397 to 4.916 ± 0.569 in Ras Al Khaimah roots ($U = 9$, Cliff's $\delta = -1.0$, $p = 0.1$), with corresponding declines in evenness at both sites (Al Ain: 0.741 ± 0.026 to 0.598 ± 0.179; Ras Al Khaimah: 0.748 ± 0.052 to 0.611 ± 0.065). Leaf communities showed higher Shannon diversity and evenness than root communities across both sites and seasons (Figure *3* A-C).

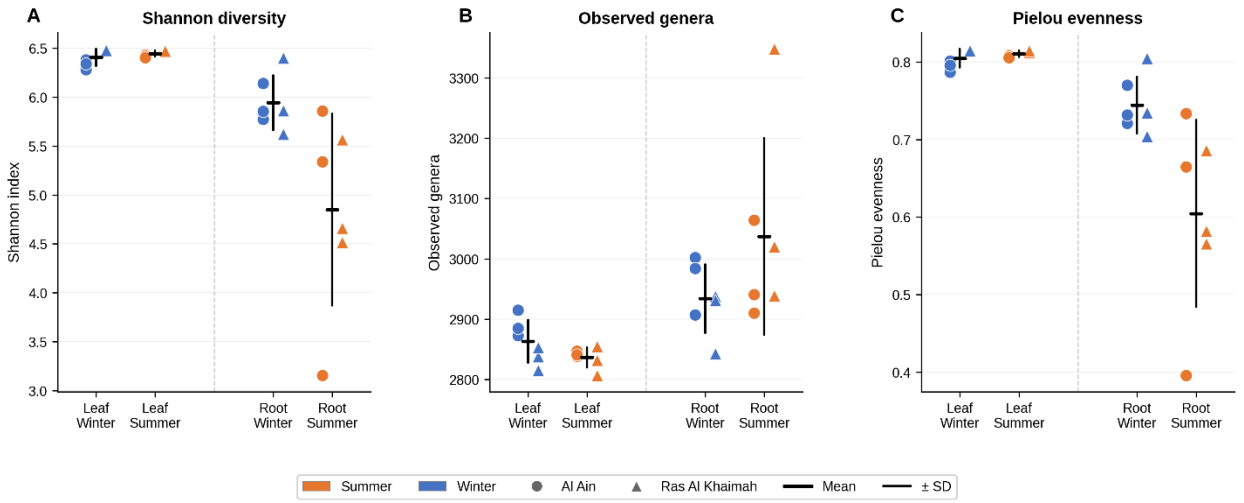

Figure 3. Alpha diversity of metagenome-derived bacterial communities across tissue types, sampling locations, and seasons. (A) Shannon diversity index, (B) observed bacterial genera, and (C) Pielou evenness. Individual points represent biological replicates (n = 3 per group); horizontal bars and error bars indicate mean ± SD. Color indicates season (orange, summer; blue, winter); marker shape indicates sampling location (circle, Al Ain; triangle, Ras Al Khaimah). Full seasonal comparison statistics are provided in Supplementary Table S1.

Beta diversity analysis based on Bray-Curtis dissimilarities confirmed substantially greater seasonal compositional turnover in root communities than in leaf communities. Winter-to-summer centroid shifts were 0.384 and 0.372 in Al Ain and Ras Al Khaimah roots respectively, compared with 0.130 and 0.040 in the corresponding leaf communities. PERMANOVA indicated moderate-to-large seasonal effects in Al Ain leaves (pseudo-F = 8.08, R^2 = 0.669, p = 0.099), Al Ain roots (pseudo-F = 2.80, R^2 = 0.412, p = 0.099), and Ras Al Khaimah roots (pseudo-F = 3.34, R^2 = 0.455, p = 0.099), while Ras Al Khaimah leaves showed a weaker seasonal effect (pseudo-F = 1.53, R^2 = 0.276, p = 0.194). Metric multidimensional scaling ordination confirmed tighter cross-seasonal clustering in leaf samples, particularly in Ras Al Khaimah, and greater seasonal separation in root samples at both sites (Figure 4A–B).

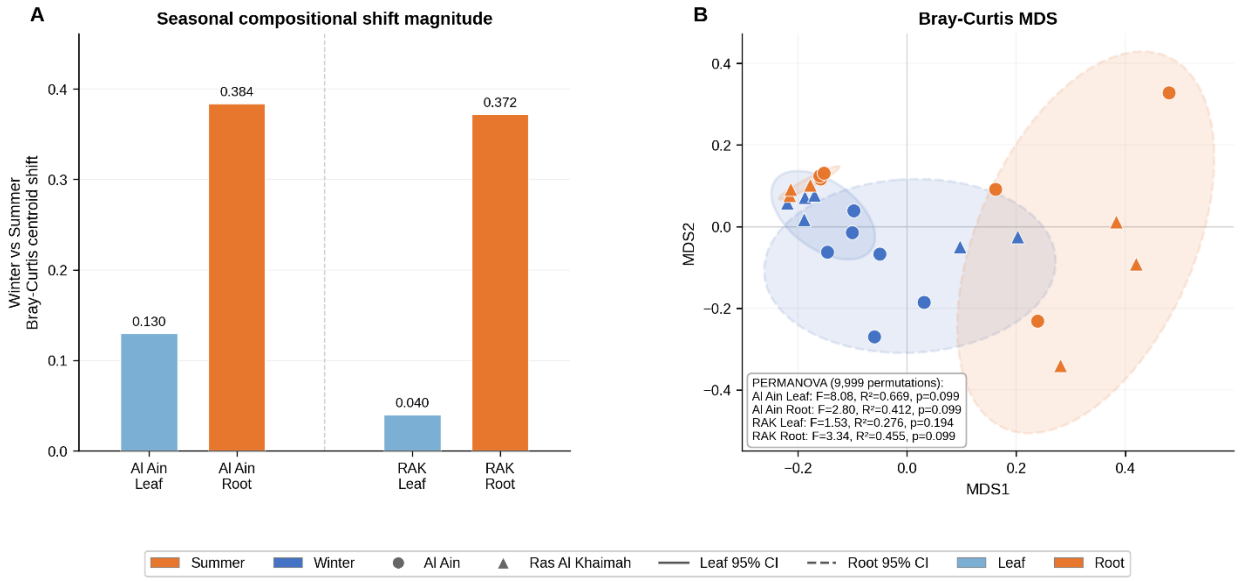

Figure 4. Seasonal compositional turnover of metagenome-derived bacterial communities across tissue types and sampling locations. (A) Winter-to-summer Bray-Curtis centroid shifts for each location–tissue subgroup. (B) Metric multidimensional scaling ordination of community composition based on Bray-Curtis dissimilarities. Dashed ellipses represent 95% confidence intervals for root communities and solid ellipses for leaf communities. PERMANOVA results (9,999 permutations) are shown in the annotation box. Color indicates season (orange, summer; blue, winter); marker shape indicates sampling location (circle, Al Ain; triangle, Ras Al Khaimah).

3.1.3. Taxonomic composition identified key taxa driving seasonal turnover across methods

At broad taxonomic levels, amplicon profiles revealed clear spatiotemporal patterns. Leaves and roots were predominantly composed of Bacteroidota and Pseudomonadota, with Actinomycetota and Bacillota at lower levels; soils were mainly dominated by Actinomycetota, Pseudomonadota, and Bacillota, while Bacteroidota and Chloroflexota varied by site and season (Figure 5). A decrease was noted in the relative abundance of Actinomycetota and Pseudomonadota from winter to summer. The abundance of Bacteroidota increased from winter to summer in Al Ain root zone samples, while the opposite was seen in the RAK root zone samples. Chloroflexota was more abundant in bulk soil than root zone soils and showed a decrease in the Al Ain root zone from winter to summer, but an increase in the RAK root zone.

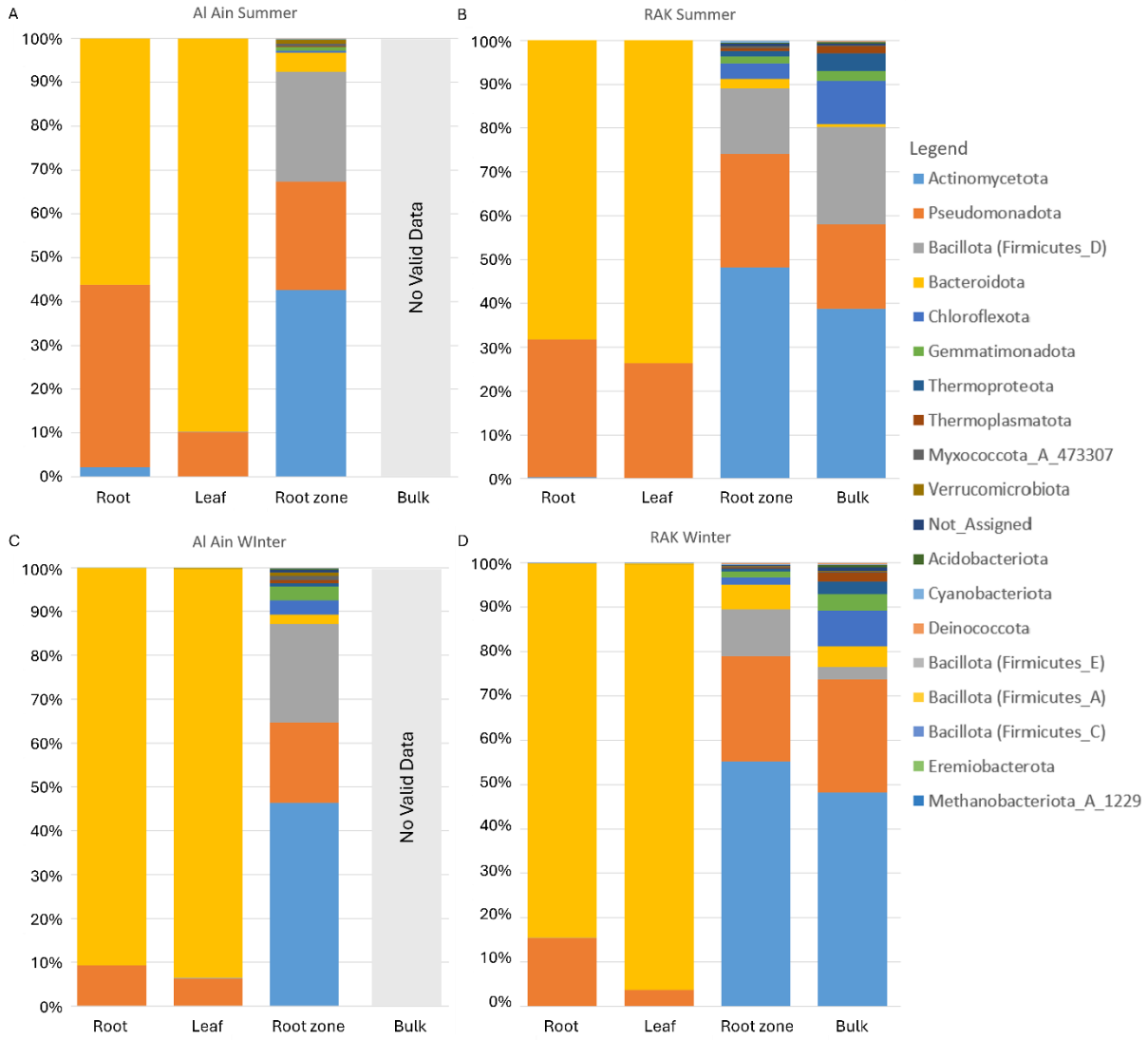

Figure 5: Seasonal Variation in the Relative Abundance of Bacterial Phyla in Al Ain and Ras Al Khaimah (RAK) Based on 16S rDNA Amplicon Data. (A, B) Relative abundance of bacterial phyla during summer in Al Ain and RAK, respectively. (C, D) Relative abundance during winter in Al Ain and RAK, respectively. Missing bulk soil samples are labeled as “No valid data.”. To note, Firmicutes are shown as two separate taxa due to the polyphyletic lineages present within the phylum in the Greengenes database reference tree. Other datasets show the phylum as a

monophyletic lineage, as per the Greengenes FAQ page (https://gtdb.ecogenomic.org/faq), and the International Code of Nomenclature of Prokaryotes (ICNP) has updated the naming conventions for prokaryotic phyla, standardizing names with the suffix "-ota" derived from the type genus (Oren & Garrity, 2021). This change had not been reflected in the Greengenes database, which still presents Bacillota as “Firmicutes” at the time of our analysis.

When examined at finer resolution, Actinomycetota orders followed the seasonal trend (Figure 6): Mycobacteriales were more abundant in summer and decreased in winter as Actinomycetales increased; Propionibacteriales in summer were offset by Coriobacteriales in winter, with root-zone soils often showing the opposite pattern (Figure 6). This example illustrates how changes within Actinobacteriota orders exhibit greater seasonal and sample type variability, highlighting the dynamic and detailed nature of community shifts that may not be as apparent when viewed only at the phylum level.

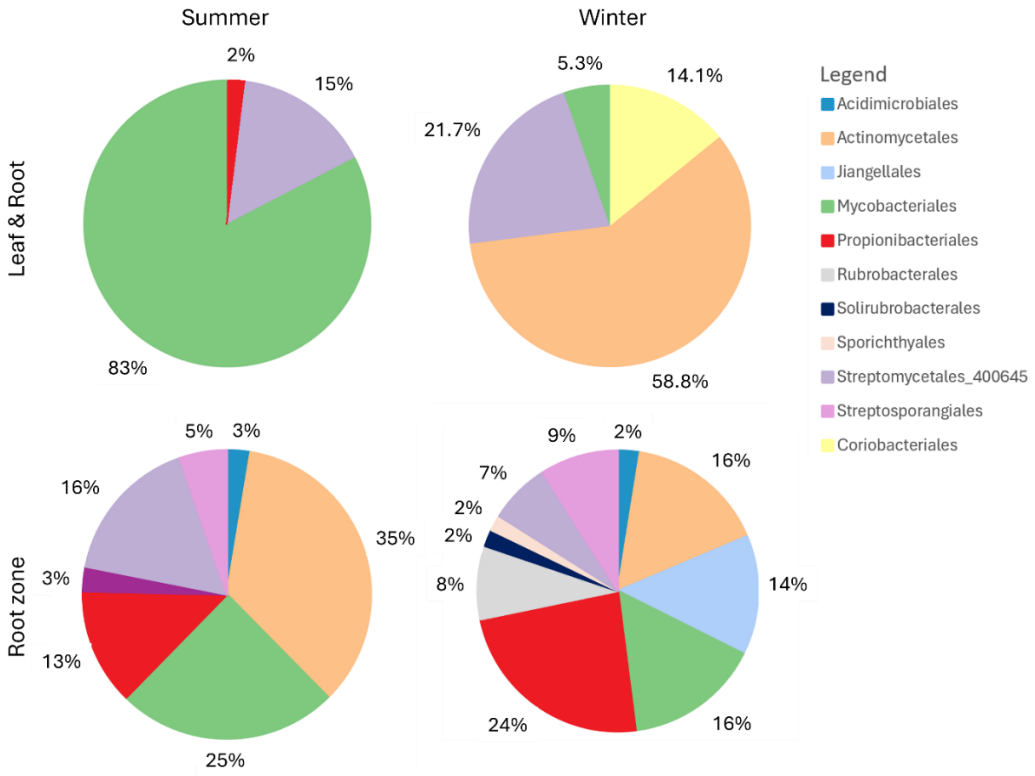

Figure 6: Seasonal variation in the relative abundance of Actinobacteriota orders across different sample types. Pie charts show the community composition of Actinobacteriota at the order level in leaf, root, and root zone soil samples during summer and winter. The charts highlight shifts in the relative abundance of dominant and minor orders across seasons and sample types.

Shotgun metagenomes confirmed the taxonomic patterns seen in the amplicon data. Shotgun metagenomic data from the same DNA as the amplicon analysis revealed that more than 50% of reads in root and leaf samples mapped to Eukaryota, whereas Bacteria dominated in soil samples (>50%). Archaea, Virus, and Fungi (inside Eukaryota) each contributed less than 1% of reads (Supplementary Figure 1). Unclassified and non-fungal Eukarya were removed to focus on relevant microbial taxa. Relative abundances were calculated from read counts for each taxonomic

group, and the top 15 phyla were highlighted by sample type, location, and season (Figure 7). Phylum-level distributions showed that Al Ain and RAK were similar within the same season, while differences between summer and winter at each site led to the clearest shifts (Figure 7). Across different sample types, Actinomycetota and Pseudomonadota were the predominant bacterial phyla (with Actinomycetota especially abundant in soil), and Ascomycota and Basidiomycota dominated fungal communities (Figure 7, 8). Archaeal compositions remained relatively stable across seasons and locations (Figure 7, 8).

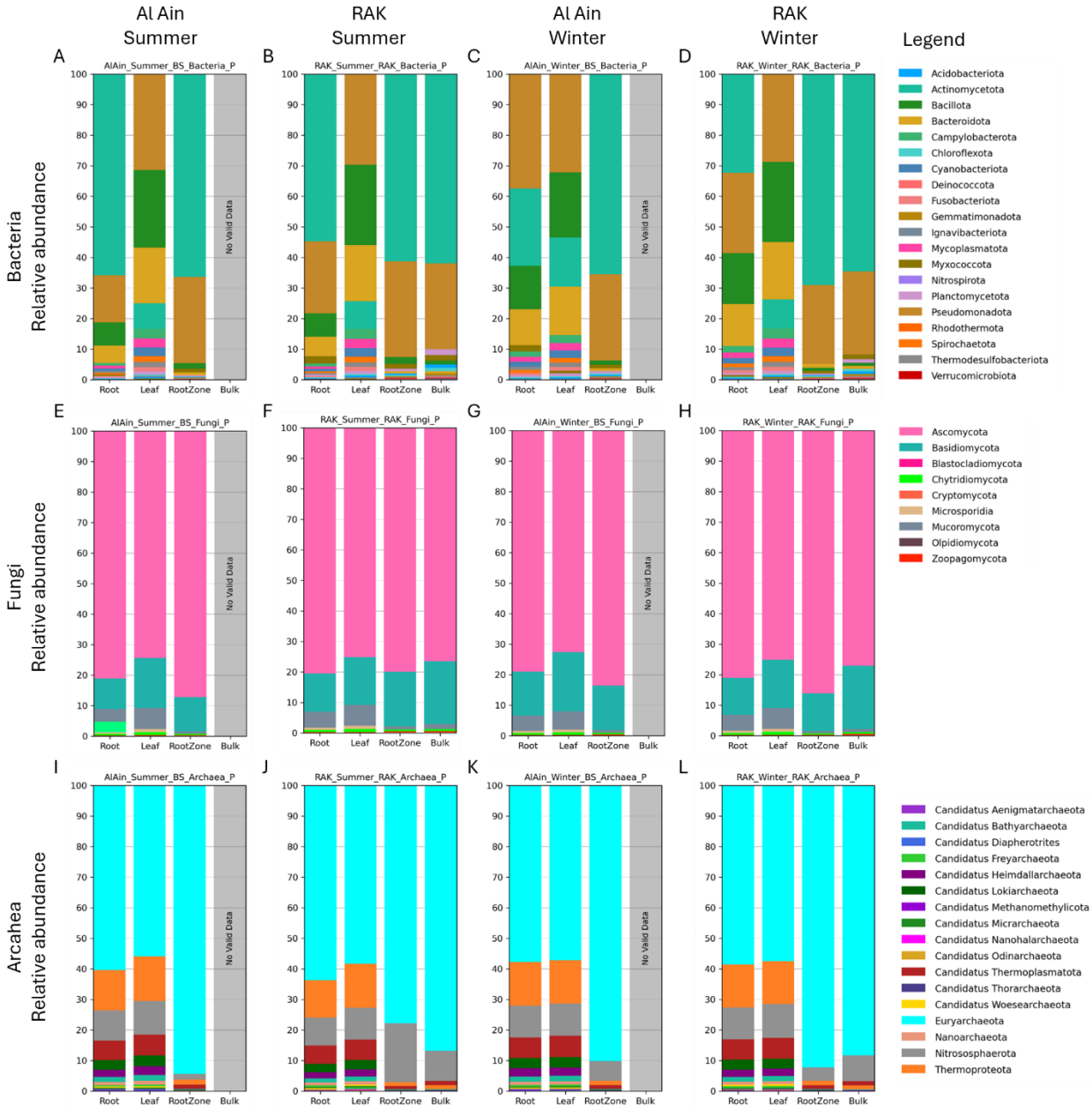

Figure 7: Phylum-level relative abundance of microbial communities in Al Ain and RAK samples based on metagenomic data. Bar graphs show the relative abundance of the top 15 bacterial (A–D), fungal (E–H), and archaeal (I–L) phyla across different sample types collected during summer and winter from Al Ain and Ras Al Khaimah (RAK). Each panel represents seasonal and site-specific variation within a specific microbial group.

At the order level (Figure 8), the highest turnover was observed in bacteria such as Pseudomonadales, Burkholderiales, Bacillales, Kitasatosporales, Pseudonocardiales, and Micrococcales. Leaves were enriched in Bacillales, along with noticeable Flavobacteriales, while roots or root-zone soils were dominated by Kitasatosporales, Pseudonocardiales, and Micrococcales. Seasonal differences were particularly evident in plant tissues: for example, Pseudonocardiales decreased from summer to winter in Al Ain roots, with winter roots showing a more uniform distribution of bacterial orders. RAK roots showed a similar trend but to a lesser extent. Fungal orders also shifted, with Pleosporales increasing from summer to winter across multiple tissues and sites, while Eurotiales decreased in Al Ain roots and Sordariales declined in Al Ain root compartments during the same period.

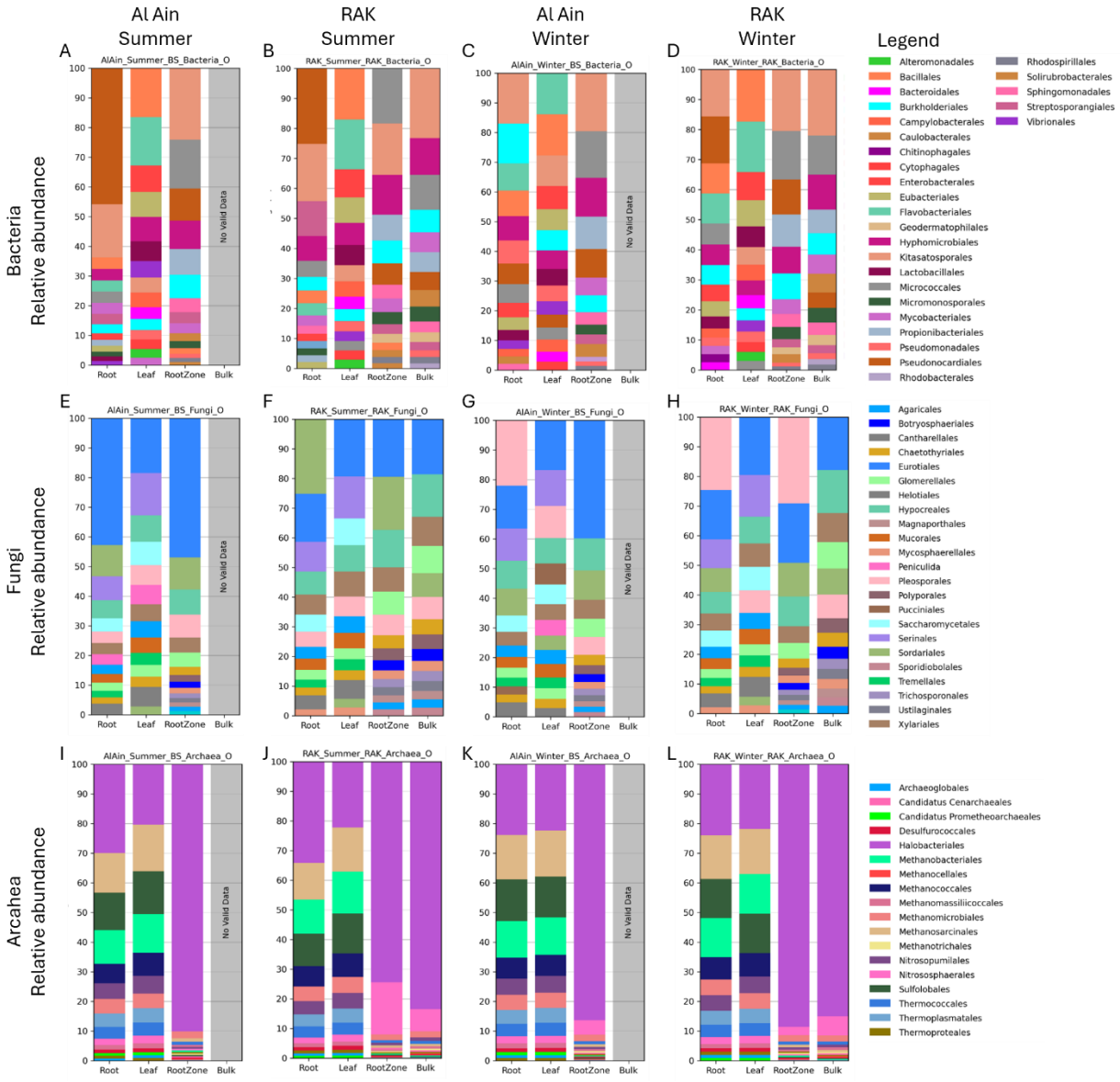

Figure 8: Order-level relative abundance of microbial communities in Al Ain and RAK samples based on metagenomic data. Bar graphs show the relative abundance of the top 15 bacterial (A–D), fungal (E–H), and archaeal (I–L) orders across different sample types collected during summer and winter from Al Ain and Ras Al Khaimah (RAK). Each panel represents seasonal and site-specific variation within a specific microbial group.

At the genus level, these order-level shifts were driven by a small number of taxa showing great directional seasonal change in root communities at both sites. Examination of the 40 most abundant

bacterial genera identified directional seasonal shifts concentrated in root communities (Supplementary Table S2). In Al Ain roots, Saccharopolyspora (log2FC = 3.91), Amycolatopsis (log2FC = 3.28), and Pseudonocardia (log2FC = 3.24) increased markedly in summer, while Pseudomonas (log2FC = −2.54) and Massilia (log2FC = −4.74) declined. In Ras Al Khaimah roots, the largest summer increases were in Nonomuraea (log2FC = 5.04), Amycolatopsis (log2FC = 1.82), and Saccharopolyspora (log2FC = 2.09), with concurrent declines in Clostridium, Vibrio, and Flavobacterium. Leaf communities showed no consistent directional shifts in dominant genera at either site (Figure 9, 10).

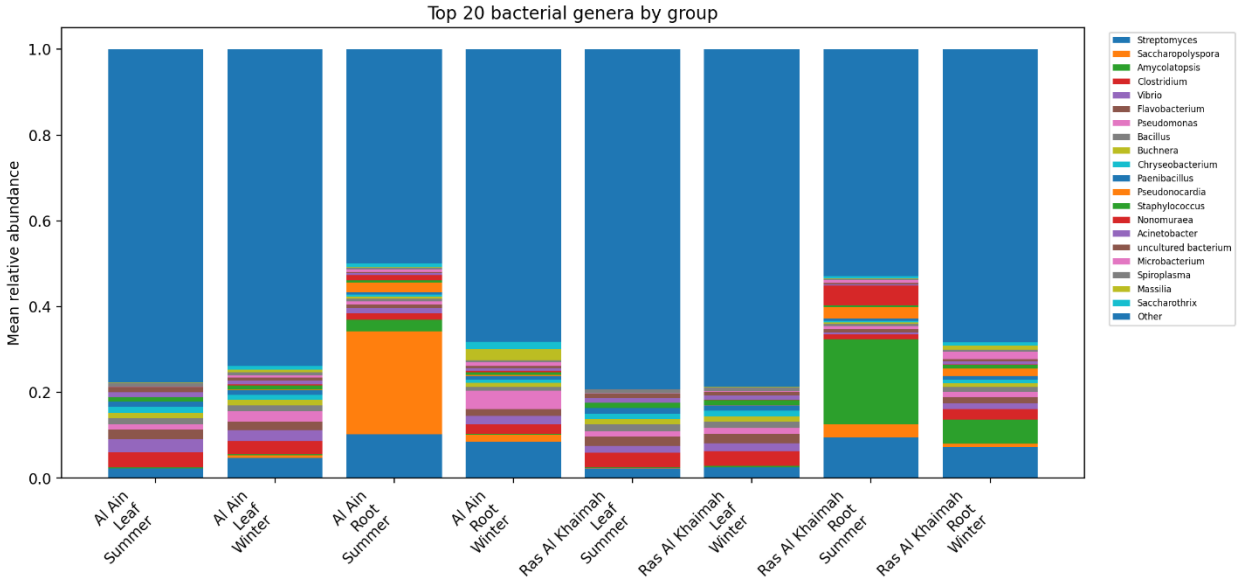

Figure 9. Mean relative abundance of the 20 most abundant bacterial genera across tissue types, sampling locations, and seasons based on metagenomic data. Each bar represents the group mean relative abundance (n = 3 biological replicates). Genera are color-coded as shown in the legend; remaining taxa are pooled as 'Other'. Full seasonal shift statistics for all 40 genera are provided in Supplementary Table S2.

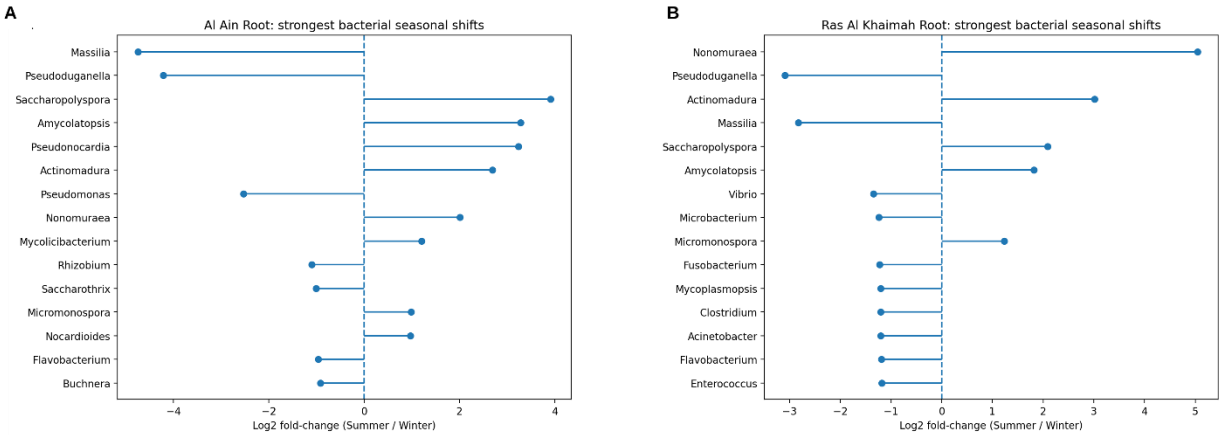

Figure 10. Seasonal log2 fold-changes in the relative abundance of dominant bacterial genera in root communities. (A) Al Ain roots and (B) Ras Al Khaimah roots. Each point represents the log2 fold-change in mean relative abundance between summer and winter (positive values indicate summer enrichment; negative values indicate winter enrichment). Only genera with the strongest directional shifts are shown; full statistics for all 40 genera are provided in Supplementary Table S2.

3.1.4. Functional profiling of root communities shows seasonal restructuring

The interpretation emphasized that the recovered taxa and pathways could contribute to the survival of *C. colocynthis*, which persists in sandy desert soils with episodic water availability and has a documented desert-adapted microbiome. Its leaf water-loss biology indicates a fast-growing, water-spender strategy rather than the highly conservative strategy seen in evergreen desert shrubs or date palm (Bueno et al., 2019; Procter et al., 2022; Elnaggar et al., 2024). All 12 libraries produced usable functional profiles after filtering. Feature recovery differed across groups, with RAK summer samples showing the highest mean numbers of mapped enzyme classes, gene families, pathways, total reads, and mapped taxa, while RAK winter samples showed the lowest mean pathway recovery and the lowest mean mapped-taxon richness (Supplementary Table 3).

After removal of unmapped and unclassified bins, the dominant named pathways were consistently central metabolic modules: branched-chain amino-acid biosynthesis, purine and guanosine

nucleotide de novo biosynthesis, the glyoxylate cycle, and TCA-associated routes (Figure 11). These functions support maintenance of biosynthetic capacity, carbon flexibility, and nucleotide turnover across all groups, rather than relying on a single stress-specialist pathway. The heatmap further showed that variation was concentrated in a subset of pathways related to nucleotide synthesis, glyoxylate/TCA metabolism, UMP biosynthesis, and fatty-acid initiation, with WBS3R and especially RAK2R driving several of the strongest sample-level deviations (Figure 12).

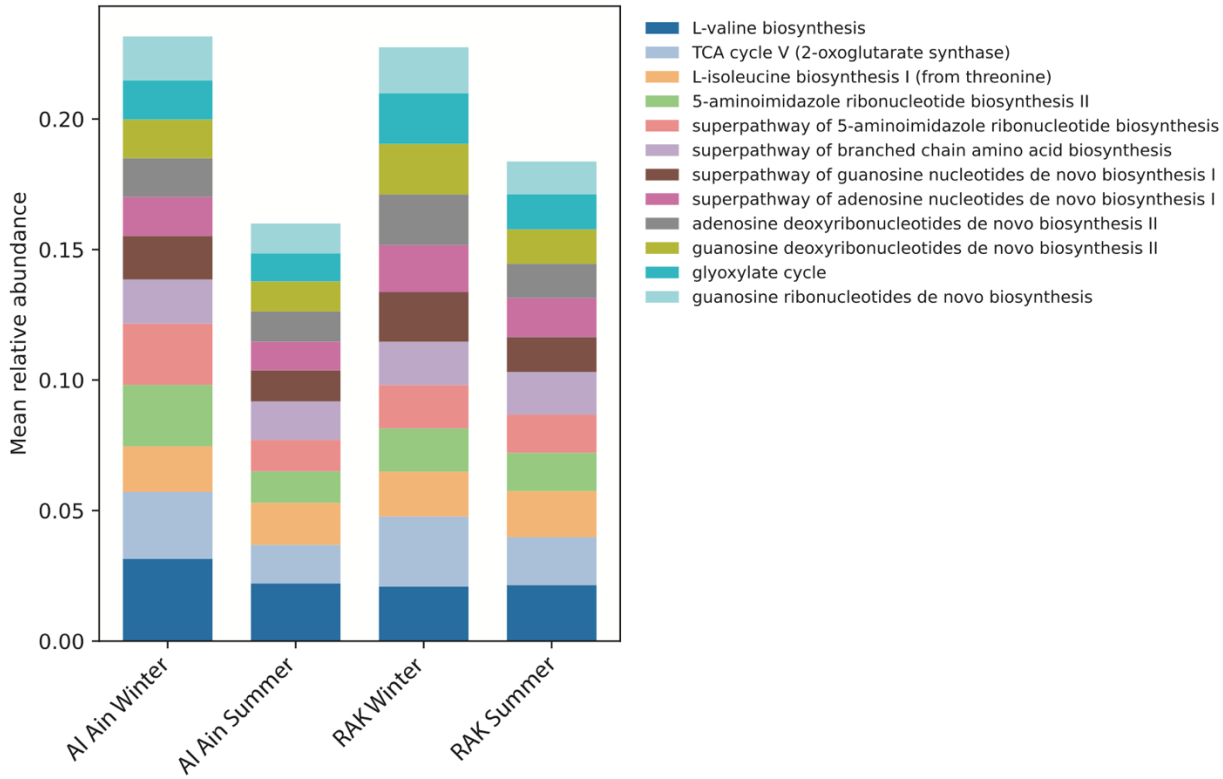

Figure 11. Mean relative abundance of the 12 most abundant mapped functional pathways in root microbial communities across sampling locations and seasons, based on HUMAnN pathway profiling. Non-informative categories (unmapped and unclassified reads) were excluded prior to analysis. Pathways are color-coded as shown in the legend.

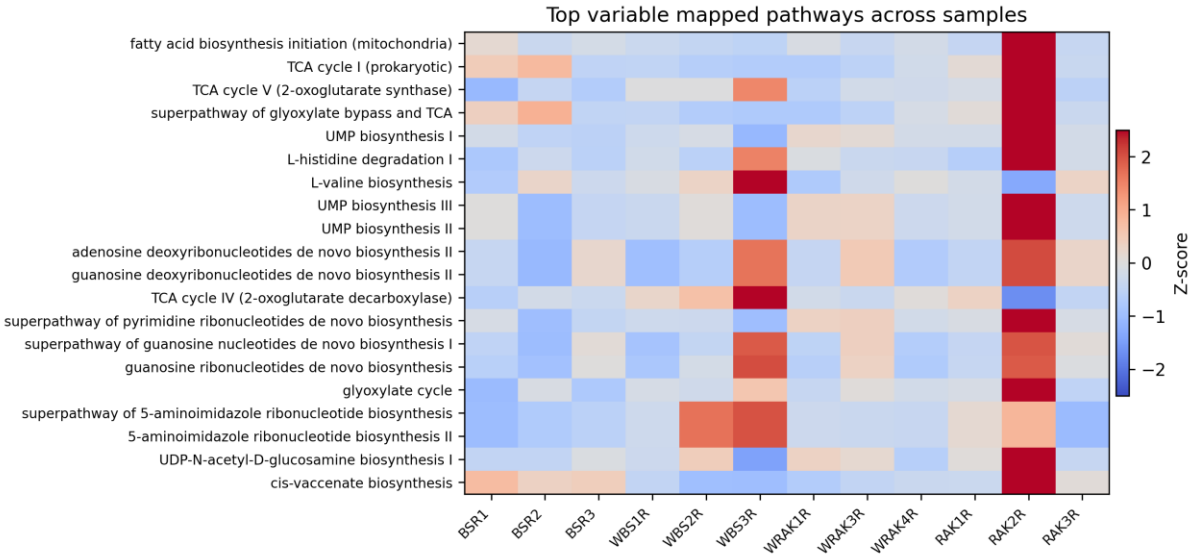

Figure 12. Heatmap of the most variable mapped functional pathways across individual root samples, based on HUMAnN pathway profiling. Values are row-scaled to highlight relative enrichment and depletion across samples. Samples are grouped by location and season; color scale indicates relative abundance after row scaling (warmer colours indicate enrichment, cooler colors indicate depletion).

Site-specific pathway contrasts were more informative when interpreted by location separately (Figure 13, Supplementary Table 4). In Al Ain roots, summer-associated pathways included colanic acid building-block biosynthesis, CMP-3-deoxy-D-manno-octulosonate biosynthesis, thiamine diphosphate biosynthesis, aspartate and asparagine biosynthesis, arginine degradation, and glucose and xylose degradation, collectively compatible with Gram-negative envelope remodeling, exopolysaccharide production, carbon scavenging, and nitrogen metabolism maintenance. Winter retained stronger signals for formaldehyde assimilation, tetrahydrofolate biosynthesis and salvage, NAD salvage, factor 420 biosynthesis, and sucrose degradation routes. In Ras Al Khaimah roots, the summer profile was characterized by central metabolism and cofactor maintenance functions, including arginine biosynthesis, glycolysis–pyruvate dehydrogenase–TCA and glyoxylate coupling, tetrahydrofolate biosynthesis and salvage, reductive TCA, NAD salvage, and formaldehyde assimilation, while winter retained comparatively higher signals for pyridoxal-

5-phosphate, menaquinol-8, polyamine, and norspermidine-associated pathways. No individual pathway passed a stringent FDR threshold, and these shifts should therefore be interpreted as coordinated functional trends rather than definitive individual biomarkers (Supplementary Table 4).

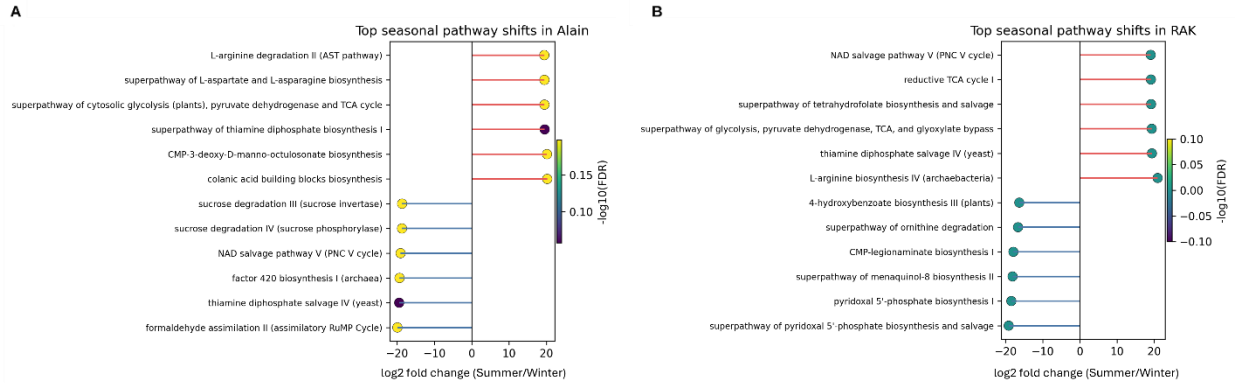

Figure 13. Site-specific seasonal pathway contrasts in root microbial communities from Al Ain (A) and Ras Al Khaimah (B), based on HUMAnN pathway profiling. Positive values indicate summer enrichment and negative values indicate winter enrichment. Pathways are ranked by effect size within each site.

Stratified HUMAnN profiles identified the candidate bacterial taxa underlying these site-specific functional shifts (Figure 14; Supplementary Table 4). In Al Ain roots, dominant functional contributors shifted from a winter signal centered on *Streptomyces griseorubens* and *Streptomyces* sp. SHP22-7 to a summer signal dominated by *Pseudomonas* taxa, particularly *P. seleniipraecipitans*, *P. zeshuii*, and *P. lutea*, with a smaller contribution from *Neorhizobium*. In Ras Al Khaimah roots, the opposite pattern emerged, with summer intensifying an actinobacterial signature centered on *Amycolatopsis methanolica*, *Streptomyces luteus*, *S. griseorubens*, and *Streptomyces* sp. SHP22-7. This site-dependent contrast indicates that summer functional adaptation in *C. colocynthis* roots is not driven by a single universal bacterial guild, with Al Ain

recruiting a Gram-negative, envelope- and exopolysaccharide-focused ensemble, while Ras Al Khaimah intensifies an actinobacterial, central-metabolism-rich consortium.

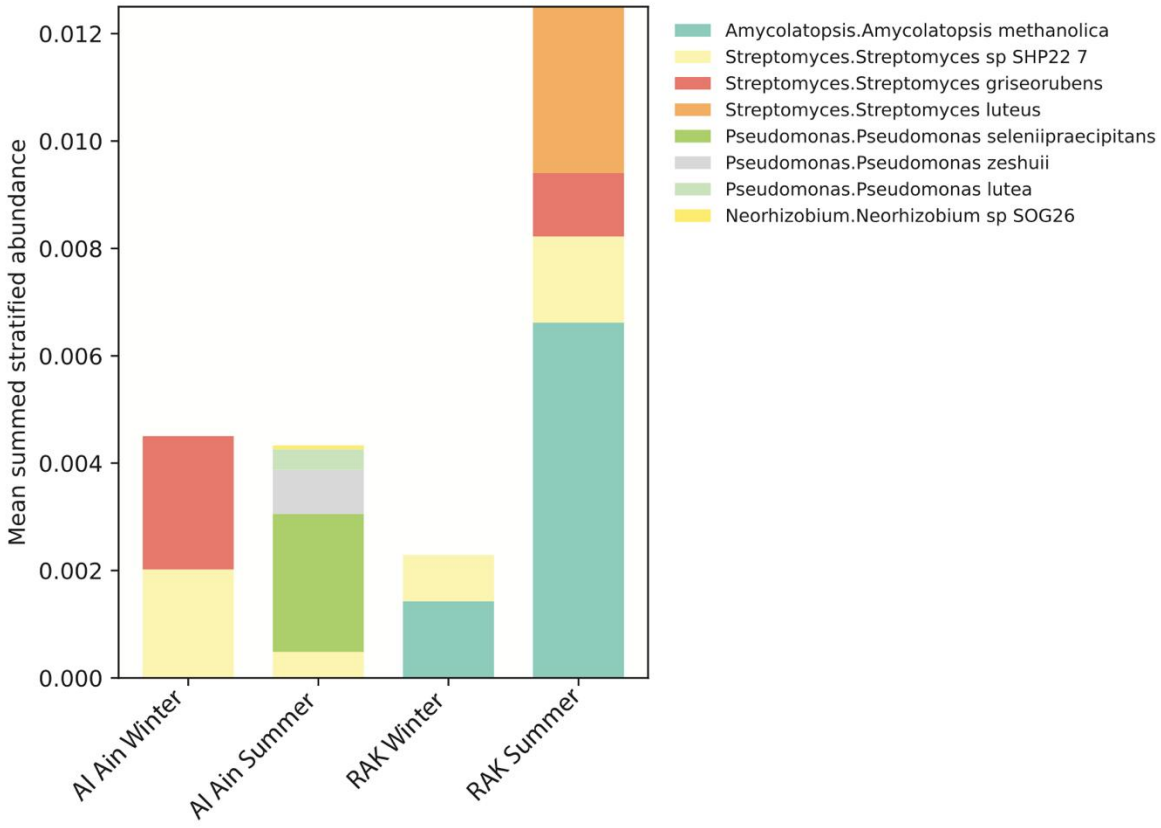

Figure 14. Mean summed stratified pathway abundance for dominant bacterial taxa contributing to functional profiles in root communities across sampling locations and seasons, based on HUMAnN stratified output. March and August correspond to winter and summer, respectively. Taxa are color-coded as shown in the legend.

3.2. Cultured isolates mirror in situ taxa and express stress-ready, plant-beneficial functions

PCR-based 16S rRNA gene sequencing classified the 24 cultured isolates into desert-associated genera, including *Bacillus* (B04, B08, B11, B12, B14, B18, B19), *Pseudomonas* (B03, B05, B06, B10, B13, B15, B17, B20, B23, B26, B27), *Plantibacter* (B07), *Paenibacillus* (B09), *Brevibacillus* (B16), *Pantoea* (B22), *Streptomyces* (B24), and *Arthrobacter* (F02). These initial identifications informed the taxonomy for subsequent assays and reflected lineages observed in the community datasets (Figure 3–6). Abiotic stress tolerance spanned multiple axes (Table 1). Several isolates maintained growth under severe osmotic stress (up to 20% PEG). Heat and salinity tolerance were limited to a few key strains: B04 and B11 grew at 55 °C; B04, B11, and B14 grew at 10% NaCl, and B11 endured 12% NaCl. Most isolates preferred pH 6–8, while B22 grew across a pH range of 4–10; multiple *Bacillus* isolates (B05, B08, B12, B18, B19) tolerated pH 6–12. These patterns suggest that resilience is distributed across different genera rather than confined to a single group lineage.

Plant growth–promoting activities were frequent but varied (Table 1). Nitrogen dissolution was observed in five *Bacillus* and two *Pseudomonas* isolates; ACC deaminase in B07, B24, and B26; cellulase in six of eleven CMC-positive isolates; amylase in eight isolates; and phosphate solubilization in ten isolates. Growth on CAS medium (siderophore screen) was common, though clearing halos were generally weak, with B20 and B27 showing the clearest zones. IAA assays showed strong positivity in B07 and B22, with mixed results in the others; LC–MS/MS confirmed the presence of multiple phytohormones (Supplementary Figure 2): Phytohormone production by bacterial isolates measured using LC-MS/MS. (A) Indole-3-acetic acid (IAA), (B) Gibberellic acid

583 (GA_3), (C) Salicylic acid (SA), (D) Abscisic acid (ABA), (E) Isopentyl adenine (iPA), and (F)
584 Indole-3-butyric acid (IBA)., with 6-BA and NAA below detection, and ABA consistently low.
585 Overall, *Bacillus* species tended to have broader enzyme capabilities and alkaline tolerance,
586 *Pseudomonas* contributed siderophore and hormone-related activity along with salt/heat tolerance,
587 and *Pantoea* combined a wide pH range with a strong IAA signal.
588

Table 1: Overview of Stress Tolerance and PGP Assay Results.

Genus	Isolate	Drought (%)	Salt (%)	Heat (°C)	pH	IAA	N dissol.	ACC Deam.	Cellulase	K sol.	Amylase	P sol.	Siderophore
Bacillus	B04	10	12	55	6-8	-	-	-	+	-	+	-	-
	B11	20*	12	55	6-8	-	-	-	+	-	+	-	-
	B14	10	10	50	6-10	-	+	-	+	-	-	-	-
	B08	0	8	45	6-12	-	+	-	-	-	+	-	-
	B12	0	6	45	6-12	-	+	-	-	-	+	-	-
	B18	0	8	45	6-12	+	+	-	+	-	+	-	-
	B19	0	8	45	6-12	+	+	-	-	-	+	-	-
Plantibacter	B07	20*	6	35	6-8	+	-	+	-	-	-	-	-
Paenibacillus	B09	0	5	45	6-8	-	-	-	-	-	+	-	-
Brevibacillus	B16	0	2	45	6-8	+	-	-	-	-	-	+	-
Pantoea	B22	20	5	40	4-10	+	-	-	+	-	-	+	-
Streptomyces	B24	20	6	45	6-8	-	-	+	+	-	+	-	-
Arthrobacter	F2	10	4	40	6-8	+	+	-	-	-	-	-	-
Pseudomonas	B03	10	2	35	6-10	-	-	-	-	+	-	+	-
	B05	20*	4	35	6-12	+	-	-	-	-	-	-	-
	B06	20	4	35	6-10	+	-	-	-	-	-	-	-
	B10	0	2	35	6-8	+	-	-	-	+	-	+	-
	B13	20*	2	35	6-10	+	-	-	-	-	-	-	-
	B15	10*	2	35	6-8	+	-	-	-	+	-	+	-

B17	0	4	35	6-10	+	-	-	-	-	-	+	-
B20	20	4	35	6-10	+	+	-	-	-	-	+	+
B23	0	2	35	6-10	-	-	+	-	+	-	-	-
B26	20	2	35	6-10	-	+	+	-	-	-	+	-
B27	10*	4	35	6-10	+	+	-	-	+	-	+	+

Whole-genome sequencing subsequently confirmed species-level identities and clarified borderline cases (Table 2, Supplementary Table 6). Species-level identification was performed by using the TYGS platform, which assigns bacterial IDs based on digital DNA-DNA hybridization (dDDH) scores. Four isolates (B08, B12, B18, B19) were initially identified as *Bacillus anthracis*. Due to the high genomic similarity among *B. anthracis*, *B. cereus*, and *B. thuringiensis* (Rasko et al., 2005), further average nucleotide identity (ANI) analysis was conducted, confirming these isolates as *B. thuringiensis*. Motility assays (not shown) on semi-solid agar supported this result, as all isolates were motile, distinguishing them from non-motile *B. anthracis*. For isolates flagged by TYGS as potential novel species (B03, B07, B17, B20, B23, B24, B26, B27, F02), ANI comparisons with the closest BLAST-matched references revealed that only B03, B23 (both *Pseudomonas*), and F02 (*Arthrobacter*) were below the 95% ANI threshold, indicating potential novel species. The remaining isolates had ANI values ≥ 95% to known species (Table 2). Genome-derived context for these culture-based traits (biosynthetic gene clusters, ortholog enrichments) is discussed in the following section.

Table 2: TYGS and OrthoANI Results for Bacterial Genomes (showing the closest relative of each isolate) and Assigned Species Identity.

Sample	16S BLAST	TYGS	Genome used for ANI	OrthoANI (%)	Species Identity	NCBI accession no.
B03	*Pseudomonas sp.*	New *Pseudomonas* sp.	*Pseudomonas thivervalensis*	93	*Pseudomonas sp.*	CP176770
B04	*Bacillus sp.*	*Bacillus licheniformis*	-	-	*Bacillus licheniformis*	CP177039
B05	*Pseudomonas sp.*	*Pseudomonas shirazensis*	-	-	*Pseudomonas shirazensis*	CP177040
B06	*Pseudomonas sp.*	*Pseudomonas shirazensis*	-	-	*Pseudomonas shirazensis*	CP177041-CP177042
B07	*Plantibacter flavus*	New *Plantibacter* sp.	*Plantibacter flavus*	95	*Plantibacter sp.*	CP177043
B08	*Bacillus sp.*	*Bacillus anthracis*	*Bacillus thurgiensis* *Bacillus cereus*	99.33 98.95	*Bacillus thuringiensis*	CP177035-CP177038

			Bacillus anthracis	98.89		
B09	*Paenibacillus lautus*	New *Paenibacillus* sp.	*Paenibacillus lautus*	98.82	*Paenibacillus lautus*	CP177044
B10	*Pseudomonas sp.*	*Pseudomonas veronii*	-	-	*Pseudomonas veronii*	CP177034
B11	*Bacillus sp.*	*Bacillus licheniformis*	-	-	*Bacillus licheniformis*	CP177045
B12	*Bacillus sp.*	*Bacillus anthracis*	*Bacillus thuringiensis*	99.1	*Bacillus thuringiensis*	CP177046
			Bacillus cereus	98.29		
			Bacillus anthracis	98.41		
B13	*Pseudomonas sp.*	*Pseudomonas shirazensis*	-	-	*Pseudomonas shirazensis*	CP177047
B14	*Bacillus sp.*	*Bacillus altitudinis*	-	-	*Bacillus altitudinis*	CP177125-CP177126

B15	*Pseudomonas sp.*	*Pseudomonas veronii*	-	-	*Pseudomonas veronii*	NZ_JBKEZL000000000
B16	*Brevibacillus sp.*	*Brevibacillus centrosporus*	-	-	*Brevibacillus centrosporus*	CP176856-CP176857
B17	*Pseudomonas sp.*	New *Pseudomonas* sp.	*Pseudomonas orientalis*	99.07	*Pseudomonas orientalis*	CP176858-CP176859
B18	*Bacillus sp.*	*Bacillus anthracis*	*Bacillus thuringiensis*	99.33	*Bacillus thuringiensis*	CP176860-CP176863
			Bacillus cereus	98.92		
			Bacillus anthracis	98.87		
B19	*Bacillus sp.*	*Bacillus anthracis*	*Bacillus thuringiensis*	99.33	*Bacillus thuringiensis*	CP176864-CP176867
			Bacillus cereus	98.93		
			Bacillus anthracis	98.87		
B20	*Pseudomonas sp.*	New *Pseudomonas* sp.	*Pseudomonas orientalis*	99.04	*Pseudomonas orientalis*	CP176868-CP176869

B22	*Pantoea sp.*	*Pantoea agglomerans*	-	-	*Pantoea agglomerans*	CP176870-CP176873
B23	*Pseudomonas sp.*	New *Pseudomonas* sp.	*Pseudomonas extremaustralis*	94.66	*Pseudomonas sp.*	CP176771
B24	*Streptomyces sp.*	New *Streptomyces* sp.	*Streptomyces mutabilis*	95.9	*Streptomyces mutabilis*	CP176874-CP176875
B26	*Pseudomonas sp.*	New *Pseudomonas* sp.	*Pseudomonas cedrina*	95.87	*Pseudomonas cedrina*	CP176793
B27	*Pseudomonas sp.*	New *Pseudomonas* sp.	*Pseudomonas orientalis*	99.12	*Pseudomonas orientalis*	CP176876-CP176877
F02	*Arthrobacter sp.*	New *Arthrobacter* sp.	*Arthrobacter nitrophenolicus*	83.99	*Arthrobacter sp.*	CP176772

3.3. Genome-resolved signals link observed phenotypes to adaptive gene content

Genome mining across the isolate set identified a consistent stress and competition toolkit that reflects the culture phenotypes discussed in the previous section. KEGG/COG profiling revealed extensive coverage of central metabolism with genus-specific features: *Pseudomonas* genomes were enriched for secondary metabolite biosynthesis, biofilm formation, and two-component systems, while *Bacillus* focused on core metabolic and cofactor pathways (Supplementary Table 7, Supplementary Figure 3). Other genera showed characteristic patterns; for example, *Streptomyces* with moderate secondary metabolism, and *Pantoea* with higher nitrogen and carbohydrate pathway signals but lower oxidative phosphorylation, aligning with niche specialization (Supplementary Table 7). Biosynthetic gene cluster (BGC) predictions supported these patterns. *Bacillus* and *Pseudomonas* contained lipopeptides (fengycin, surfactin, lichenysin, viscosin) linked to pathogen suppression (Guo et al., 2014; Ahmad et al., 2023), while classical antibiotic BGCs (meilingmycin, microansamycin, lankacidin) were found in *Streptomyces* and *Bacillus*. Multiple siderophores (pyoverdine, bacillibactin, petrobactin, schizokinen) indicated iron acquisition under limitation (Ravel and Cornelis, 2003). Stress-related loci included ectoine (e.g., B09, B16, B24) and carotenoid-associated clusters (e.g., B05, B06, B07, B13, B22, B24, B26), reflecting drought/oxidative protection themes seen in vitro (Supplementary Table 8) (Uarrota et al., 2018; Richter et al., 2019). OrthoVenn3 showed isolate-specific enrichments relevant to function: benzoate catabolism in B12, phosphonate metabolism in B23, and pyoverdine biosynthesis in B20, matching its siderophore activity in culture (Supplementary Table 9, Supplementary Figure 5-7).

A pangenome analysis using our B20 genome and other publicly available *P. orientalis* genomes (Supplementary Table 10) demonstrated an open pangenome ($\gamma = 0.3313$), with presence/absence matrices distinguishing core from accessory modules (Figure 15A–B). Plant-associated genomes contained more lineage-specific accessory-intermediate genes than their free-living counterparts (Figure 15C), and several of these plant-associated accessory genes mapped to tryptophan-linked pathways, including tryptophan 2-monooxygenase (IAM pathway toward IAA) and tryptophan decarboxylase (tryptamine route), supporting hormone-related activities observed in culture (e.g., isolate B20) (Supplementary Figure 8, 9). Conversely, free-living strains showed greater nucleotide diversity ($\pi = 0.021$) compared to plant-associated strains ($\pi = 0.016$; $P < 0.005$) (Figure 15D), reflecting broader environmental exposure and gene flow. Lifestyle-related accessory genes also revealed a competition signal in free-living genomes absent from the plant-associated set: genes providing protection against bacteriocins, including a colicin-E3 immunity protein, were found among free-living isolates (Supplementary Figure 8, 9), indicating adaptation to microbe–microbe antagonism outside the host. Alongside the tryptophan-derived modules in plant-associated strains, these differences suggest that accessory content aligns with ecological needs: host interaction versus environmental competition within *P. orientalis*.

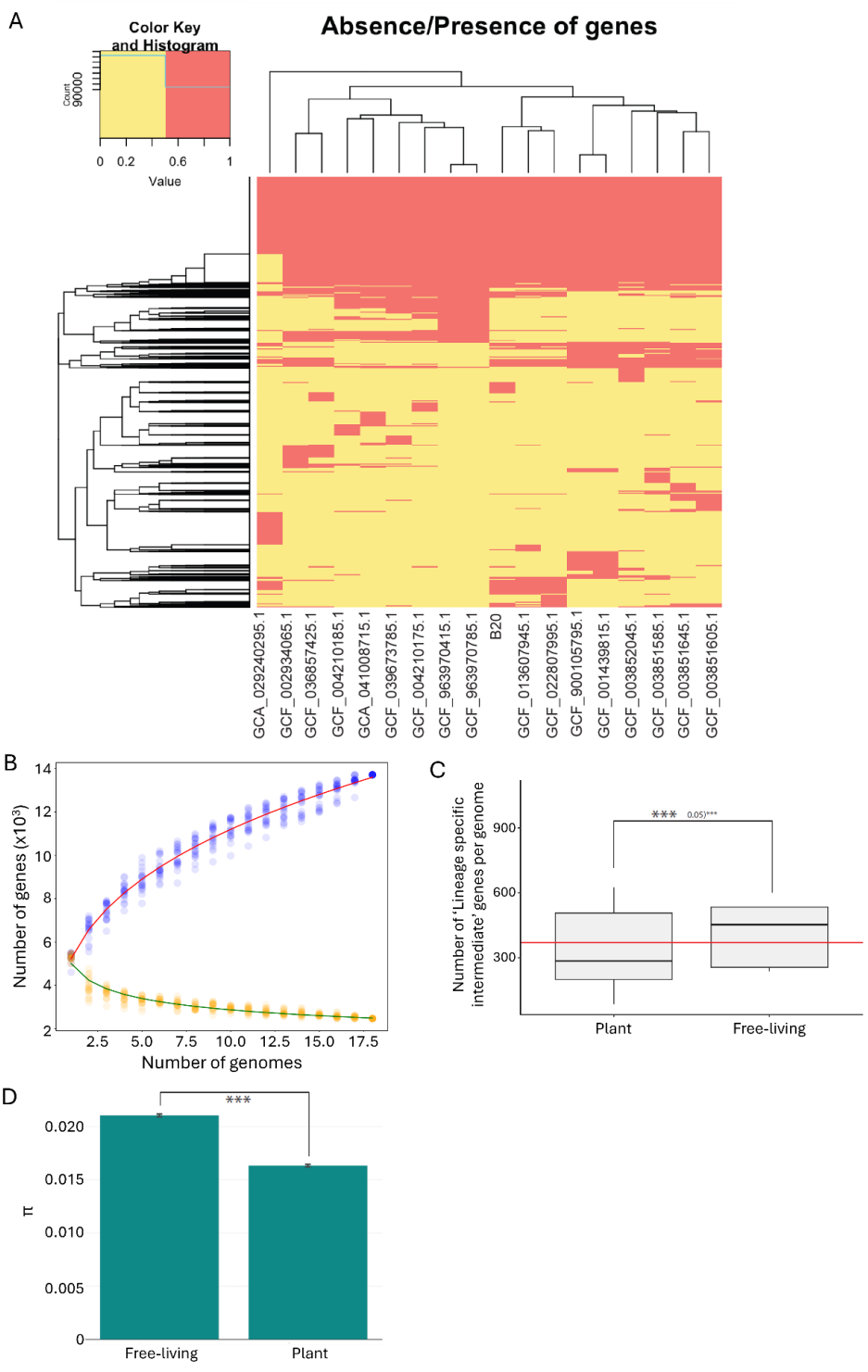

Figure 15: Pangenome analysis of *Pseudomonas orientalis* reveals an open pan-genome and distinct differences between plant-associated and free-living strains. (A) Heatmap displays gene presence (Rodriguez and Redman) and absence (yellow) across genomes, including isolate B20,

with hierarchical clustering of core and accessory genes. (B) Curves show gene counts as genomes increase, with fitted trend lines indicating sustained gene acquisition ($\gamma = 0.3313$). (C) Bar plot compares lineage-specific accessory genes per genome, with higher counts in plant-associated strains. (D) Nucleotide diversity (π) is higher in free-living strains ($\pi = 0.021$) than in plant-associated strains ($\pi = 0.016$), indicating greater pan-genome fluidity.

4. Discussion

This study aimed to explain how the microbiome helps *Citrullus colocynthis* survive in dry environments. It placed the results within desert holobionts and combined detailed community profiling with culture-based traits to explore how seasonal changes relate to stress-related functions. Unlike previous work on *C. colocynthis* that focused mainly on cultures or had limited geographic and temporal scope, this research combines amplicon and shotgun surveys across two UAE regions with isolate phenotypes and genome analyses, allowing us to connect seasonal community shifts to traits and genes in representative strains.

Analysis of 16S amplicon data revealed notable seasonal effects on plant endophytic communities (Figure 1). Species richness decreased significantly from winter to summer in both leaf and root endospheres, while Shannon diversity showed a tissue-specific pattern: root communities were more diverse in summer, whereas leaf communities showed no significant change in evenness despite reduced richness. NMDS ordination confirmed strong seasonal structuring of community composition, with season accounting for 71.9% of beta diversity variation (PERMANOVA: $R^2 = 0.719$, $p = 0.0008$), tissue type explaining a further significant proportion ($R^2 = 0.179$, $p = 0.041$),

and sampling location having no significant effect ($p = 0.806$). Soil communities remained stable across seasons in both alpha and beta diversity (Figure 2), consistent with soil acting as a more stable microbial reservoir than plant endospheric compartments (Edwards et al., 2018; Eida et al., 2018).

Metagenomic profiling corroborated these patterns while adding resolution that clarifies apparent discrepancies between the two datasets (Figure 5, 6). Leaf communities showed no meaningful seasonal change in any diversity metric at either site, consistent with the amplicon findings. Root communities showed the strongest seasonal signal in both datasets, with Bray-Curtis centroid shifts in roots substantially exceeding those in leaves and PERMANOVA confirming moderate-to-large seasonal effects at both sites. The direction of root Shannon diversity differed between methods — increasing in the amplicon data but decreasing in the metagenome — reflecting their different resolutions rather than a genuine contradiction. The amplicon captures greater evenness among the reduced pool of summer-persistent taxa, while the metagenome captures the broader shift toward dominance by a small number of actinobacterial genera. Together, the two datasets describe the same ecological event from a complementary perspective.

Phylum-level amplicon profiles reflect seasonal contrasts between plant compartments and soils, with Bacteroidota and Pseudomonadota dominating leaves and roots, and Actinomycetota and Pseudomonadota prominent in soils (Figure 5). These patterns extended down the taxonomic hierarchy: within Actinomycetota, Actinomycetales and Coriobacteriales were enriched in winter, whereas Mycobacteriales and Propionibacteriales were more common in summer (Figure *6*). Consistent with these 16S patterns, shotgun metagenomes showed Actinomycetota and

Pseudomonadota as the predominant bacterial phyla, with within-site seasonal shifts in plant tissues but comparatively steady soils (Figure *7*). They also captured order-level turnover in Pseudomonadales, Burkholderiales, Bacillales, Kitasatosporales, Pseudonocardiales, and Micrococcales, with Pseudonocardiales notably decreasing from summer to winter in Al Ain roots (Figure 8). At the genus level, this order-level restructuring was driven by the marked summer expansion of *Saccharopolyspora*, *Amycolatopsis*, *Pseudonocardia*, and *Nonomuraea* in root communities at both sites, concurrent with declines in *Pseudomonas*, *Massilia*, *Flavobacterium*, and *Clostridium* (Figure 7, 8). These genera are frequently associated with stress tolerance, secondary metabolism, and persistence under dry or nutrient-limited conditions (Compant et al., 2019; Ali et al., 2022b), and leaf communities showed no equivalent directional restructuring at either site. Fungal orders also changed seasonally, with winter increases in Pleosporales and a persistent presence of Eurotiales, while archaeal and viral components remained relatively stable in space and time (Figure 5–6). Similar host-linked adaptability against a more stable soil environment has been reported in desert halophytes, cacti along aridity gradients, and in native Arabian flora, where host identity strongly influences endosphere composition (Eida et al., 2018; Karray et al., 2020; Khan et al., 2022; Mousa et al., 2024).

Beyond taxonomic restructuring, shotgun metagenomic pathway profiling provided insight into the functional consequences of these seasonal community shifts. Despite the absence of a statistically significant overall four-group effect in the pathway PERMANOVA, functional profiles did not simplify in summer — pathway diversity rose modestly at both sites in summer, and the dominant pathways remained centered on amino acid biosynthesis, purine synthesis, glyoxylate shunts, and TCA-linked functions. This pattern is consistent with summer survival in

C. colocynthis roots being supported by maintenance of metabolic breadth rather than contraction into a narrow stress response (Elnaggar et al., 2024) and aligns with prior characterization of this species as hosting a structured desert microbiome rather than a randomly assembled one (Procter et al., 2022).

The site-dependent shift in functional carriers has clear biological relevance. In Al Ain, the summer recruitment of plant-beneficial *Pseudomonas* taxa is ecologically meaningful: members of this genus are well documented for exopolysaccharide production, biofilm formation, ACC-deaminase-mediated stress buffering, siderophore production, and reinforcement of root barriers under drought and heat (Morcillo and Manzanera, 2021; Zhang and White, 2021; Mehmood et al., 2023; Zboralski and Filion, 2023). The matching Al Ain summer pathway signal (colanic acid and CMP-KDO biosynthesis, thiamine diphosphate, aspartate and asparagine biosynthesis, and glucose and xylose degradation) aligns with Gram-negative envelope investment, carbon scavenging, and anabolic maintenance. In Ras Al Khaimah, the summer intensification of *Amycolatopsis methanolica* and multiple *Streptomyces* taxa points to a different strategy. Endophytic actinobacteria are repeatedly associated with drought and heat adaptation, secondary metabolite production, and root growth promotion in stressful habitats (Singh and Dubey, 2018; Zhang and White, 2021), and the matching RAK summer pathways (arginine biosynthesis, tetrahydrofolate biosynthesis and salvage, reductive TCA, NAD salvage, and formaldehyde assimilation) align with redox management, cofactor economy, and biosynthetic persistence rather than envelope protection.

These contrasting functional strategies reflect the broader biology of *C. colocynthis,* whose life strategy creates pressure for below-ground buffering during hot, dry periods, and the present data suggest that this buffering is achieved through two distinct, site-specific endophytic consortia: a pseudomonad-rich, exopolysaccharide-centered ensemble in Al Ain and an actinobacterial, cofactor- and central-metabolism-centered consortium in Ras Al Khaimah. Despite these compositional differences, both strategies converge on the same functional outcome: maintenance of root metabolic activity and stress buffering under summer arid conditions, suggesting that *C. colocynthis* selects for functional capacity rather than taxonomic identity when assembling its summer endophytic community.

Functional specialization explains this plasticity. *In silico* signals and *in vitro* traits both pointed to stress-protectant pathways, phytohormones, and biosynthetic gene clusters (BGCs). Lipopeptide and siderophore BGCs in *Pseudomonas orientalis* (B17, B20, B27) and *Bacillus licheniformis* (B04) matched with tolerance to drought, salinity, and heat, as well as plant growth–promoting (PGP) activity (Table 1, Supplementary Table 8). Additional functions, including phytohormone production, phosphate solubilization, and siderophore biosynthesis, were seen in *Paenibacillus lautus* (B09) and *Streptomyces mutabilis* (B24), among others. Genes for ectoine and carotenoids support osmotic and oxidative stress protection, as seen in arid environments (Guo et al., 2014; Uarrota et al., 2018; Richter et al., 2019; Ahmad et al., 2023). This pattern aligns with broader evidence that desert microbiomes favor salt and heat-tolerant communities with metabolites that help hosts thrive under water stress and high temperatures (Glick, 2012; Backer et al., 2018; Alsharif et al., 2020).

Genome-resolved analysis refined these connections. The *P. orientalis* pangenome was open, with distinct core–accessory divisions (Figure 15). Plant-associated genomes contained accessory genes linked to tryptophan pathways for IAA, including tryptophan 2-monooxygenase (IAM pathway) and tryptophan decarboxylase (tryptamine route), which matched culture-level IAA signals and known *Pseudomonas* adaptations (Loper et al., 2012; Li et al., 2018; Saati-Santamaría et al., 2022; Tang et al., 2023b). In contrast, free-living genomes exhibited higher nucleotide diversity and included competition-related factors, like a colicin-E3 immunity protein that was absent from the plant-associated group (Supplementary Figure 9), aligning with selective pressures in open environments. Altogether, these differences indicate that accessory genome content reflects ecological demands, like host interaction versus environmental competition, within a single species.

The ecological and practical implications are outlined below. The connection between seasonal community shifts (Figure 7, 8), isolated phenotypes (Table 1), and genome-inferred capabilities highlights potential microbiome-aware strategies for arid conditions. Stress-tolerant, growth-promoting bacteria can boost nutrient uptake and crop yields while reducing input requirements in saline or drought-prone environments (Glick, 2012; Backer et al., 2018). Regional experience from the Arabian Peninsula, including the UAE, supports this potential: desert plant systems produce endophytes with high salt tolerance and measurable plant growth-promoting effects in crops, creating a pipeline from native flora to bioinoculants (Eida et al., 2018; Gairola et al., 2018; Alsharif et al., 2020; Mousa et al., 2024). In this context, *C. colocynthis* not only serves as a model for understanding desert holobionts but also as a source of strong strains with potential for practical applications.

519

520 Our design prioritized a broad scope and the integration of community surveys with culture-based
521 work. Therefore, metagenomes were analyzed for their composition rather than pathway
522 reconstruction, and taxonomic classifications naturally depend on database choice and classifier
523 thresholds. Amplicon profiling (V3–V4) provides robust community patterns but, by design, has
524 region-specific biases and limited strain-level resolution. Building on this foundation,
525 transcriptomics and metabolomics would test whether key genes and clusters are active under
526 plant-relevant conditions, and controlled *in planta* experiments would establish causal effects on
527 host performance. Expanded bulk-soil sampling and longer time series could improve the contrast
528 between soil stability and plant-driven turnover. Finally, targeted evaluation of highlighted strains
529 (*e.g., representatives of B. licheniformis and P. orientalis)* under field-relevant stress conditions
530 provides a practical next step toward developing bioinoculants for desert agriculture.

531

532 This study builds on a previously published single-season, single-location pilot characterization of
533 the *C. colocynthis* endophytic microbiome (Procter et al., 2022) which identified a structured,
534 biologically interesting microbial community and provided the rationale for expanding sampling
535 to two sites and two seasons in the present work. The primary limitation of the current study is the
536 modest number of biological replicates (n = 3 per location–tissue–season subgroup), reflecting its
537 role as an expanded exploratory baseline for an understudied desert holobiont. Prior to sequencing,
538 three technical replicates per biological sample were pooled to maximize community
539 representativeness within each data point. Statistical interpretation therefore relies on effect sizes,
540 multivariate patterns, and directional consistency rather than taxon-level adjusted p-values. Where
541 the two sequencing approaches converge, namely stronger seasonal turnover in roots than in leaves

and summer enrichment of actinobacterial genera, conclusions are reinforced by cross-method agreement. Where they diverge, most notably in the direction of change in root Shannon diversity, the discrepancy reflects methodological differences in taxonomic resolution and sensitivity to dominant taxa rather than a biological contradiction, as discussed above.

A further limitation concerns the relationship between the cultured isolate collection and the metagenomic community profiles. The taxa driving the main seasonal story in the metagenome, particularly *Saccharopolyspora*, *Amycolatopsis*, *Nonomuraea*, and the *Pseudomonas* taxa dominant in Al Ain summer roots, are not well represented among the cultured isolates characterized in this study. This gap is common in culture-based microbiome work, where the most ecologically abundant or functionally active taxa are frequently the least amenable to standard cultivation conditions (Liu et al., 2021; Nauwynck et al., 2025). The cultured collection, therefore, provides complementary functional and genomic resolution for the taxa it does capture, but should not be interpreted as representative of the dominant metagenomic community. Future work combining targeted isolation strategies, such as dilution-to-extinction or in situ cultivation approaches, with the metagenomic profiles generated here would help close this gap. Taken together, the findings should be considered hypothesis-generating, pending validation in larger cohorts and cultivation approaches informed by the dominant taxa identified here.

5. Conclusion

Across two regions in the UAE and different seasons, the *Citrullus colocynthis* holobiont shows evidence of a microbiome that reorganizes under environmental pressure in a consistent and ecologically coherent manner; an adaptive “intelligence” expressed through changes in community membership and the selective retention of stress-relevant functions. By combining spatiotemporal

community profiling across amplicon and metagenomic resolution with cultured representatives and genome-level context, this work establishes a clear framework that links who is present, what they can do, and how those abilities are distributed across different lifestyles. These foundations directly point to practical applications. Stress-tolerant, growth-promoting taxa, their functional pathway repertoires, and their gene inventories offer accessible entry points for microbiome-aware strategies in arid agriculture, from targeted inoculants and consortium design to screening pipelines based on desert-native diversity. More broadly, the dataset and framework provided here form the backbone for future studies that incorporate expression and metabolite evidence, test causal effects in plants, and translate desert holobiont principles into resilient, sustainable food systems.

6. List of abbreviations

ABA	Abscisic Acid
ACC	1-aminocyclopropane-1-carboxylate
ANI	Average Nucleotide Identity
ASV	Amplicon Sequence Variant
BGCs	Biosynthetic Gene Clusters
BUSCO	Benchmarking Universal Single-Copy Orthologs
CAS	Chrome azurol S
CFUs	Colony Forming Units
CMC	Carboxymethyl cellulose
COG	Cluster of orthologous gene
dDDH	Digital DNA-DNA Hybridization
DF	Dworkin and Foster
GA_3	Gibberellic Acid
GO	Gene Ontology
IAA	Indole-3-Acetic Acid
IBA	Indole-3-Butyric Acid
ICNP	International Code of Nomenclature of Prokaryotes
IDs	Identities
iPA	Isopentyl Adenine
ITS	Internal Transcribed Spacer Region
KEGG	Kyoto Encyclopedia of Genes and Genomes
KO	KEGG Orthology

LB	Luria-Bertani
LC-MS/MS	Liquid chromatography-mass spectrometry/mass spectrometry
NA	Nutrient Agar
NMDS	Non-Metric Multidimensional Scaling
ONT	Oxford Nanopore Technologies
PCoA	Principal Coordinates Analysis
PDA	Potato Dextrose Agar
PDB	Potato Dextrose Broth
PE	Paired-End
PEG	Polyethylene Glycol
PGP	Plant Growth Promoting
PGPR	Plant Growth Promoting Rhizobacteria
RAK	Ras Al Khaimah
ROS	Reactive Oxygen Species
SA	Salicylic Acid
SNA	Starch Nitrate Agar
TYGS	Type (Strain) Genome Server
w/v	Weight per volume
WGS	Whole Genome Sequencing

7. Declarations

7.1. Authors' contributions

Conceptualization and study design: KMH, KMAA; Methodology (Sample collection & processing): MP, BK, SA, FH, KA, IS, KMH, and KMAA; Analysis (Data curation): MP, NS, KMH, and KMAA; Funding acquisition: KMAA, KMH; Writing original draft: MP and KMH; Writing, review and editing: All.

7.2. Acknowledgements

The authors would like to thank and acknowledge the United Arab Emirates University (UAEU; Al Ain, UAE) and the Khalifa Center for Genetic Engineering and Biotechnology (KCGEB; Al Ain, UAE) for providing laboratory facilities and additional resources.

7.3. Conflicts of interest

The authors declare that they have no conflicts of interest. The funders had no role in the study's design, data collection, analysis, interpretation, manuscript writing, or the decision to publish the results.

7.4. Funding

This research was funded by the United Arab Emirates University Program for Advanced Research (UPAR) grant (Fund number 31S438).

7.5. Availability of data and materials

The sequencing data generated for bacterial genomes during this study have been deposited in the NCBI-SRA database under the Bioproject ID: PRJNA1199959 and PRJNA1199998. The metagenome (16s amplicon (V3-V4)) data generated during this study have been submitted to the NCBI-SRA database under the BioProject id: PRJNA1345893.

References

(IPCC), I.P.o.C.C. (2023) Summary for Policymakers. In *Climate Change 2023: Synthesis Report*. Core Writing Team, H.L.a.J.R. (ed). IPCC, Geneva, Switzerland, pp. 1-34.

Abushamleh, N.H., El-Keblawy, A., Mosa, K.A., Soliman, S.S.M., and Tsombou, F.M. (2022) Different Traits Affect Salinity and Drought Tolerance during Germination of *Citrullus colocynthis*, a Potential Cash Crop in Arid Lands. *Seeds* **1**: 244-259.

Ahmad, T., Xing, F., Nie, C., Cao, C., Xiao, Y., Yu, X. et al. (2023) Biocontrol potential of lipopeptides produced by the novel *Bacillus subtilis* strain Y17B against postharvest *Alternaria* fruit rot of cherry. *Front Microbiol* **14**: 1150217.

Al-Shuaibi, B.K., Kazerooni, E.A., Hussain, S., Velazhahan, R., and Al-Sadi, A.M. (2023) Plant-Disease-Suppressive and Growth-Promoting Activities of Endophytic and Rhizobacterial Isolates Associated with *Citrullus colocynthis*. *Pathogens* **12**: 1275.

Ali, A.R., Bahrami, Y., Kakaei, E., Mohammadzadeh, S., Bouk, S., and Jalilian, N. (2022a) Isolation and identification of endophytic actinobacteria from *Citrullus colocynthis* (L.) Schrad and their antibacterial properties. *Microb Cell Fact* **21**: 206.

Ali, S., Tyagi, A., Park, S., Mir, R.A., Mushtaq, M., Bhat, B. et al. (2022b) Deciphering the plant microbiome to improve drought tolerance: Mechanisms and perspectives. *Environmental and Experimental Botany* **201**: 104933.

Alsharif, W., Saad, M.M., and Hirt, H. (2020) Desert Microbes for Boosting Sustainable Agriculture in Extreme Environments. *Front Microbiol* **11**: 1666.

Anderson, M.J. (2001) A new method for non-parametric multivariate analysis of variance. *Austral Ecology* **26**: 32-46.

Andrews, S. (2010). FastQC: A Quality Control Tool for High Throughput Sequence Data [Online]. URL http://www.bioinformatics.babraham.ac.uk/projects/fastqc/

Argiroff William, A., Carrell Alyssa, A., Klingeman Dawn, M., Dove Nicholas, C., Muchero, W., Veach Allison, M. et al. (2024) Seasonality and longer-term development generate temporal dynamics in the Populus microbiome. *mSystems* **9**: e00886-00823.

Backer, R., Rokem, J.S., Ilangumaran, G., Lamont, J., Praslickova, D., Ricci, E. et al. (2018) Plant Growth-Promoting Rhizobacteria: Context, Mechanisms of Action, and Roadmap to Commercialization of Biostimulants for Sustainable Agriculture. *Front Plant Sci* **9**: 1473.

Beghini, F., McIver, L.J., Blanco-Míguez, A., Dubois, L., Asnicar, F., Maharjan, S. et al. (2021) Integrating taxonomic, functional, and strain-level profiling of diverse microbial communities with bioBakery 3. *Elife* **10**.

Blin, K., Shaw, S., Augustijn, H.E., Reitz, Z.L., Biermann, F., Alanjary, M. et al. (2023) antiSMASH 7.0: new and improved predictions for detection, regulation, chemical structures and visualisation. *Nucleic Acids Res* **51**: W46-W50.

Bolger, A.M., Lohse, M., and Usadel, B. (2014) Trimmomatic: a flexible trimmer for Illumina sequence data. *Bioinformatics* **30**: 2114-2120.

635 Bray, J.R., and Curtis, J.T. (1957) An Ordination of the Upland Forest Communities of Southern
636 Wisconsin. *Ecological Monographs* **27**: 325-349.
637 Bueno, A., Alfarhan, A., Arand, K., Burghardt, M., Deininger, A.-C., Hedrich, R. et al. (2019)
638 Effects of temperature on the cuticular transpiration barrier of two desert plants with water-
639 spender and water-saver strategies. *Journal of Experimental Botany* **70**: 1613-1625.
640 Chao, A. (1984) Nonparametric Estimation of the Number of Classes in a Population.
641 *Scandinavian Journal of Statistics* **11**: 265-270.
642 Compant, S., Samad, A., Faist, H., and Sessitsch, A. (2019) A review on the plant microbiome:
643 Ecology, functions, and emerging trends in microbial application. *Journal of Advanced*
644 *Research* **19**: 29-37.
645 Dane, F., Liu, J., and Zhang, C. (2006) Phylogeography of the Bitter Apple, Citrullus Colocynthis.
646 *Genetic Resources and Crop Evolution* **54**: 327-336.
647 De Vrieze, M., Varadarajan, A.R., Schneeberger, K., Bailly, A., Rohr, R.P., Ahrens, C.H., and
648 Weisskopf, L. (2020) Linking Comparative Genomics of Nine Potato-Associated
649 Pseudomonas Isolates With Their Differing Biocontrol Potential Against Late Blight.
650 *Frontiers in Microbiology* **Volume 11 - 2020**.
651 Dekak, A., Menasria, T., Mekahlia, M.N., and Chenchouni, H. (2025) Soil–plant–microbiome
652 interactions in drylands: soil bacteria isolated from the rhizosphere of a xerophytic plant
653 gather multiple plant growth promoting properties. *Euro-Mediterranean Journal for*
654 *Environmental Integration*.
655 Dworkin, M., and Foster, J.W. (1958) Experiments with some microorganisms which utilize
656 ethane and hydrogen. *J Bacteriol* **75**: 592-603.
657 Edwards, J.A., Santos-Medellín, C.M., Liechty, Z.S., Nguyen, B., Lurie, E., Eason, S. et al. (2018)
658 Compositional shifts in root-associated bacterial and archaeal microbiota track the plant
659 life cycle in field-grown rice. *PLOS Biology* **16**: e2003862.
660 Eida, A.A., Ziegler, M., Lafi, F.F., Michell, C.T., Voolstra, C.R., Hirt, H., and Saad, M.M. (2018)
661 Desert plant bacteria reveal host influence and beneficial plant growth properties. *PLoS*
662 *One* **13**: e0208223.
663 Elmahi, Y., Alshamsi Mohammed, S., Sudalaimuthuasari, N., Kundu, B., AlMaskari Raja, S.,
664 Hazzouri Khaled, M. et al. (2021) Complete Genome Sequences of Pseudomonas
665 atacamensis Strain SM1 and Pseudomonas toyotomiensis Strain SM2, Isolated from the
666 Date Palm Rhizosphere. *Microbiology Resource Announcements* **10**: 10.1128/mra.00253-
667 00221.
668 Elnaggar, A., Tsombou, F.M., Hussain, M.I., Almehdi, A.M., Abideen, Z., Yong, J.W.H., and El-
669 Keblawy, A. (2024) Citrullus colocynthis regulates photosynthetic and biochemical
670 processes to develop stress resilience and sustain growth under sub-optimal temperatures.
671 *Plant Stress* **12**: 100502.
672 Ewens, W.J., and Grant, G.R. (2001) Blast. In *Statistical Methods in Bioinformatics*. New York,
673 NY: Springer New York, pp. 269-302.

674 Franzosa, E.A., McIver, L.J., Rahnavard, G., Thompson, L.R., Schirmer, M., Weingart, G. et al.
675 (2018) Species-level functional profiling of metagenomes and metatranscriptomes. *Nat*
676 *Methods* **15**: 962-968.
677 Gairola, S., Al Shaer, K.I., Al Harthi, E.K., and Mosa, K.A. (2018) Strengthening desert plant
678 biotechnology research in the United Arab Emirates: a viewpoint. *Physiol Mol Biol Plants*
679 **24**: 521-533.
680 Glick, B.R. (2012) Plant growth-promoting bacteria: mechanisms and applications. *Scientifica*
681 *(Cairo)* **2012**: 963401.
682 Glick, B.R., and Gamalero, E. (2021) Recent Developments in the Study of Plant Microbiomes.
683 *Microorganisms* **9**: 1533.
684 Guo, Q., Dong, W., Li, S., Lu, X., Wang, P., Zhang, X. et al. (2014) Fengycin produced by Bacillus
685 subtilis NCD-2 plays a major role in biocontrol of cotton seedling damping-off disease.
686 *Microbiol Res* **169**: 533-540.
687 Hall, T.A. (1999) BioEdit: a user-friendly biological sequence alignment editor and analysis
688 program for Windows 95/98/NT. In *Nucleic acids symposium series*: Oxford, pp. 95-98.
689 Hassani, M.A., Duran, P., and Hacquard, S. (2018) Microbial interactions within the plant
690 holobiont. *Microbiome* **6**: 58.
691 Horesh, G., Taylor-Brown, A., McGimpsey, S., Lassalle, F., Corander, J., Heinz, E., and Thomson,
692 N.R. (2021) Different evolutionary trends form the twilight zone of the bacterial pan-
693 genome. *Microb Genom* **7**.
694 Howe, A., Stopnisek, N., Dooley, S.K., Yang, F., Grady, K.L., and Shade, A. (2023) Seasonal
695 activities of the phyllosphere microbiome of perennial crops. *Nat Commun* **14**: 1039.
696 Hussain, A.I., Rathore, H.A., Sattar, M.Z., Chatha, S.A., Sarker, S.D., and Gilani, A.H. (2014)
697 *Citrullus colocynthis* (L.) Schrad (bitter apple fruit): a review of its phytochemistry,
698 pharmacology, traditional uses and nutritional potential. *J Ethnopharmacol* **155**: 54-66.
699 Karray, F., Gargouri, M., Chebaane, A., Mhiri, N., Mliki, A., and Sayadi, S. (2020) Climatic
700 Aridity Gradient Modulates the Diversity of the Rhizosphere and Endosphere Bacterial
701 Microbiomes of Opuntia ficus-indica. *Front Microbiol* **11**: 1622.
702 Khan, A.L., Lopes, L.D., Bilal, S., Asaf, S., Crawford, K.M., Balan, V. et al. (2022) Microbiome
703 Variation Across Populations of Desert Halophyte Zygophyllum qatarensis. *Front Plant*
704 *Sci* **13**: 841217.
705 Kimbrel, J.A., Jeffrey, B.M., and Ward, C.S. (2022) Prokaryotic Genome Annotation. *Methods*
706 *Mol Biol* **2349**: 193-214.
707 Korneliussen, T.S., Albrechtsen, A., and Nielsen, R. (2014) ANGSD: Analysis of Next Generation
708 Sequencing Data. *BMC Bioinformatics* **15**: 356.
709 Landesman, W.J., Freedman, Z.B., and Nelson, D.M. (2019) Seasonal, sub-seasonal and diurnal
710 variation of soil bacterial community composition in a temperate deciduous forest. *FEMS*
711 *Microbiol Ecol* **95**.

Li, J., Zhang, L., Yao, G., Zhu, L., Lin, J., Wang, C. et al. (2022) Synergistic effect of co-culture rhizosphere *Streptomyces*: A promising strategy to enhance antimicrobial activity and plant growth-promoting function. *Front Microbiol* **13**: 976484.

Li, M., Guo, R., Yu, F., Chen, X., Zhao, H., Li, H., and Wu, J. (2018) Indole-3-Ace{Li, 2018 #1248}tic Acid Biosynthesis Pathways in the Plant-Beneficial Bacterium Arthrobacter pascens ZZ21. *Int J Mol Sci* **19**.

Liu, X., Wang, M., Nie, Y., and Wu, X.-L. (2021) Isolation Chip Increases Culturable Bacterial Diversity and Reduces Cultivation Bias. *Current Microbiology* **78**: 2025-2032.

Loper, J.E., Hassan, K.A., Mavrodi, D.V., Davis, E.W., II, Lim, C.K., Shaffer, B.T. et al. (2012) Comparative Genomics of Plant-Associated Pseudomonas spp.: Insights into Diversity and Inheritance of Traits Involved in Multitrophic Interactions. *PLOS Genetics* **8**: e1002784.

Lu, Y., Zhou, G., Ewald, J., Pang, Z., Shiri, T., and Xia, J. (2023) MicrobiomeAnalyst 2.0: comprehensive statistical, functional and integrative analysis of microbiome data. *Nucleic Acids Res* **51**: W310-W318.

Matthews, C.A., Watson-Haigh, N.S., Burton, R.A., and Sheppard, A.E. (2024) A gentle introduction to pangenomics. *Brief Bioinform* **25**.

McDonald, D., Jiang, Y., Balaban, M., Cantrell, K., Zhu, Q., Gonzalez, A. et al. (2024) Greengenes2 unifies microbial data in a single reference tree. *Nat Biotechnol* **42**: 715-718.

Mehmood, N., Saeed, M., Zafarullah, S., Hyder, S., Rizvi, Z.F., Gondal, A.S. et al. (2023) Multifaceted Impacts of Plant-Beneficial Pseudomonas spp. in Managing Various Plant Diseases and Crop Yield Improvement. *ACS Omega* **8**: 22296-22315.

Mesny, F., Hacquard, S., and Thomma, B.P.H.J. (2023) Co-evolution within the plant holobiont drives host performance. *EMBO Rep* **24**: e57455.

Meybodi, M.S.K. (2020) A Review on Pharmacological Activities of Citrullus colocynthis (L.) Schrad. *Asian Journal of Research and Reports in Endocrinology* **3**: 25–34.

Morcillo, R.J.L., and Manzanera, M. (2021) The Effects of Plant-Associated Bacterial Exopolysaccharides on Plant Abiotic Stress Tolerance. *Metabolites* **11**.

Moriya, Y., Itoh, M., Okuda, S., Yoshizawa, A.C., and Kanehisa, M. (2007) KAAS: an automatic genome annotation and pathway reconstruction server. *Nucleic Acids Res* **35**: W182-185.

Mousa, W.K., Abu-Izneid, T., and Salah-Tantawy, A. (2024) High-throughput sequencing reveals the structure and metabolic resilience of desert microbiome confronting climate change. *Frontiers in Plant Science* **Volume 15 - 2024**.

Nauwynck, W., Sakarika, M., Faust, K., and Boon, N. (2025) Differential recovery of chain-elongating bacteria: comparing droplet, plating, and dilution-to-extinction methods. *mSystems* **10**: e01356-01325.

Noor, S.O., Al-Zahrani, D.A., Hussein, R.M., Baeshen, M.N., Moussa, T.A.A., Abo-Aba, S.M. et al. (2021) Assessment of fungal diversity in soil rhizosphere associated with Rhazya stricta and some desert plants using metagenomics. *Arch Microbiol* **203**: 1211-1219.

Page, A.J., Cummins, C.A., Hunt, M., Wong, V.K., Reuter, S., Holden, M.T. et al. (2015) Roary: rapid large-scale prokaryote pan genome analysis. *Bioinformatics* **31**: 3691-3693.

752 Pielou, E.C. (1966) The measurement of diversity in different types of biological collections.
753 *Journal of Theoretical Biology* **13**: 131-144.
754 Procter, M., Kundu, B., Sudalaimuthuasari, N., AlMaskari, R.S., Saeed, E.E., Hazzouri, K.M., and
755 Amiri, K.M.A. (2022) Microbiome of Citrullus colocynthis (L.) Schrad. Reveals a
756 Potential Association with Non-Photosynthetic Cyanobacteria. *Microorganisms* **10**: 2083.
757 R Core Team (2024) R: A Language and Environment for Statistical Computing. In. Vienna,
758 Austria: R Foundation for Statistical Computing.
759 Rasko, D.A., Altherr, M.R., Han, C.S., and Ravel, J. (2005) Genomics of the Bacillus cereus group
760 of organisms. *FEMS Microbiol Rev* **29**: 303-329.
761 Ravel, J., and Cornelis, P. (2003) Genomics of pyoverdine-mediated iron uptake in pseudomonads.
762 *Trends Microbiol* **11**: 195-200.
763 Richter, A.A., Mais, C.N., Czech, L., Geyer, K., Hoeppner, A., Smits, S.H.J. et al. (2019)
764 Biosynthesis of the Stress-Protectant and Chemical Chaperon Ectoine: Biochemistry of the
765 Transaminase EctB. *Front Microbiol* **10**: 2811.
766 Rodriguez, R., and Redman, R. (2008) More than 400 million years of evolution and some plants
767 still can't make it on their own: plant stress tolerance via fungal symbiosis. *J Exp Bot* **59**:
768 1109-1114.
769 Saati-Santamaría, Z., Baroncelli, R., Rivas, R., and García-Fraile, P. (2022) Comparative
770 Genomics of the Genus Pseudomonas Reveals Host- and Environment-Specific Evolution.
771 *Microbiol Spectr* **10**: e0237022.
772 Sahu, P.K., Tilgam, J., Mishra, S., Hamid, S., Gupta, A., K., J. et al. (2022) Surface sterilization
773 for isolation of endophytes: Ensuring what (not) to grow. *Journal of Basic Microbiology*
774 **62**: 647-668.
775 Seppey, M., Manni, M., and Zdobnov, E.M. (2019) BUSCO: Assessing Genome Assembly and
776 Annotation Completeness. *Methods Mol Biol* **1962**: 227-245.
777 Shah, A., Nazari, M., Antar, M., Msimbira, L.A., Naamala, J., Lyu, D. et al. (2021) PGPR in
778 Agriculture: A Sustainable Approach to Increasing Climate Change Resilience. *Frontiers*
779 *in Sustainable Food Systems* **5**.
780 Shannon, C.E. (1948) A Mathematical Theory of Communication. *Bell System Technical Journal*
781 **27**: 379-423.
782 Silva, J., and Hussain, A. (2017) Citrullus colocynthis (L.) Schrad. (colocynth): Biotechnological
783 perspectives. *Emirates Journal of Food and Agriculture* **29**: 83.
784 Singh, R., and Dubey, A.K. (2018) Diversity and Applications of Endophytic Actinobacteria of
785 Plants in Special and Other Ecological Niches. *Frontiers in Microbiology* **Volume 9 -**
786 **2018**.
787 Sohrabi, M., Samsampour, D., and Bagheri, A. (2024) Molecular Identification of Fungal
788 Endophytes of Medicinal Plant Citrullus colocynthis (L.) Schrad as a Medicinal Plant: Role
789 of Tissue Type and Sampling Location on the Diversity. *Mol Biotechnol* **66**: 424-431.

790 Sun, J., Lu, F., Luo, Y., Bie, L., Xu, L., and Wang, Y. (2023) OrthoVenn3: an integrated platform
791 for exploring and visualizing orthologous data across genomes. *Nucleic Acids Res* **51**:
792 W397-W403.
793 Tang, J., Li, Y., Zhang, L., Mu, J., Jiang, Y., Fu, H. et al. (2023a) Biosynthetic Pathways and
794 Functions of Indole-3-Acetic Acid in Microorganisms. *Microorganisms* **11**.
795 Tang, J., Li, Y., Zhang, L., Mu, J., Jiang, Y., Fu, H. et al. (2023b) Biosynthetic Pathways and
796 Functions of Indole-3-Acetic Acid in Microorganisms. *Microorganisms* **11**: 2077.
797 Tatusova, T., DiCuccio, M., Badretdin, A., Chetvernin, V., Nawrocki, E.P., Zaslavsky, L. et al.
798 (2016) NCBI prokaryotic genome annotation pipeline. *Nucleic Acids Res* **44**: 6614-6624.
799 Uarrota, V.G., Stefen, D.L.V., Leolato, L.S., Gindri, D.M., and Nerling, D. (2018) Revisiting
800 Carotenoids and Their Role in Plant Stress Responses: From Biosynthesis to Plant
801 Signaling Mechanisms During Stress. In *Antioxidants and Antioxidant Enzymes in Higher*
802 *Plants*. Gupta, D.K., Palma, J.M., and Corpas, F.J. (eds). Cham: Springer International
803 Publishing, pp. 207-232.
804 UniProt, C. (2023) UniProt: the Universal Protein Knowledgebase in 2023. *Nucleic Acids Res* **51**:
805 D523-D531.
806 Vandenkoornhuyse, P., Quaiser, A., Duhamel, M., Le Van, A., and Dufresne, A. (2015) The
807 importance of the microbiome of the plant holobiont. *New Phytol* **206**: 1196-1206.
808 Walker, B.J., Abeel, T., Shea, T., Priest, M., Abouelliel, A., Sakthikumar, S. et al. (2014) Pilon:
809 an integrated tool for comprehensive microbial variant detection and genome assembly
810 improvement. *PLoS One* **9**: e112963.
811 Wick, R.R., Judd, L.M., Gorrie, C.L., and Holt, K.E. (2017) Unicycler: Resolving bacterial
812 genome assemblies from short and long sequencing reads. *PLoS Comput Biol* **13**:
813 e1005595.
814 Wood, D.E., Lu, J., and Langmead, B. (2019) Improved metagenomic analysis with Kraken 2.
815 *Genome Biol* **20**: 257.
816 Yoon, S.H., Ha, S.M., Lim, J., Kwon, S., and Chun, J. (2017) A large-scale evaluation of
817 algorithms to calculate average nucleotide identity. *Antonie Van Leeuwenhoek* **110**: 1281-
818 1286.
819 Zboralski, A., and Filion, M. (2023) Pseudomonas spp. can help plants face climate change.
820 *Frontiers in Microbiology* **Volume 14 - 2023**.
821 Zhang, Q., and White, J.F. (2021) Bioprospecting Desert Plants for Endophytic and Biostimulant
822 Microbes: A Strategy for Enhancing Agricultural Production in a Hotter, Drier Future.
823 *Biology (Basel)* **10**.
824 Zhang, Y., Du, Y., Zhang, Z., Islam, W., and Zeng, F. (2024) Unveiling the diversity, composition,
825 and dynamics of phyllosphere microbial communities in Alhagi sparsifolia across desert
826 basins and seasons in Xinjiang, China. *Frontiers in Microbiology* **Volume 15 - 2024**.
827 Zimin, A.V., Marcais, G., Puiu, D., Roberts, M., Salzberg, S.L., and Yorke, J.A. (2013) The
828 MaSuRCA genome assembler. *Bioinformatics* **29**: 2669-2677.